AD-A098 896 NAVAL RESEARCH LAB WASHINGTON DC F/G 20/8
AN INITIAL STUDY OF THE INJECTION OF AN INTENSE RELATIVISTIC EL--ETC(U)
MAR 81 R B FIORITO, R F FERNSLER, J R GREIG
UNCLASSIFIED NRL-MR-4405 NL

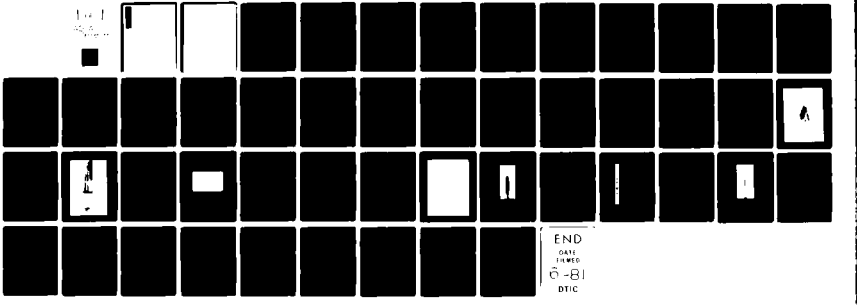

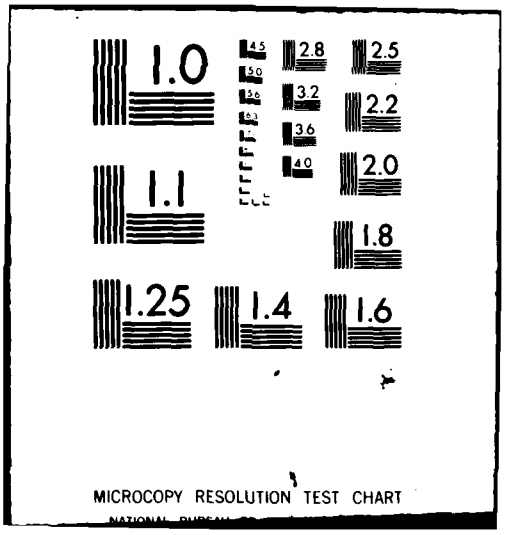
1.0
1.1
1.25
1.4
1.6
1.8
2.0
2.2
2.5
2.8
3.2
3.6
4.0
4.5
5.0
5.6
MICROCOPY RESOLUTION TEST CHART

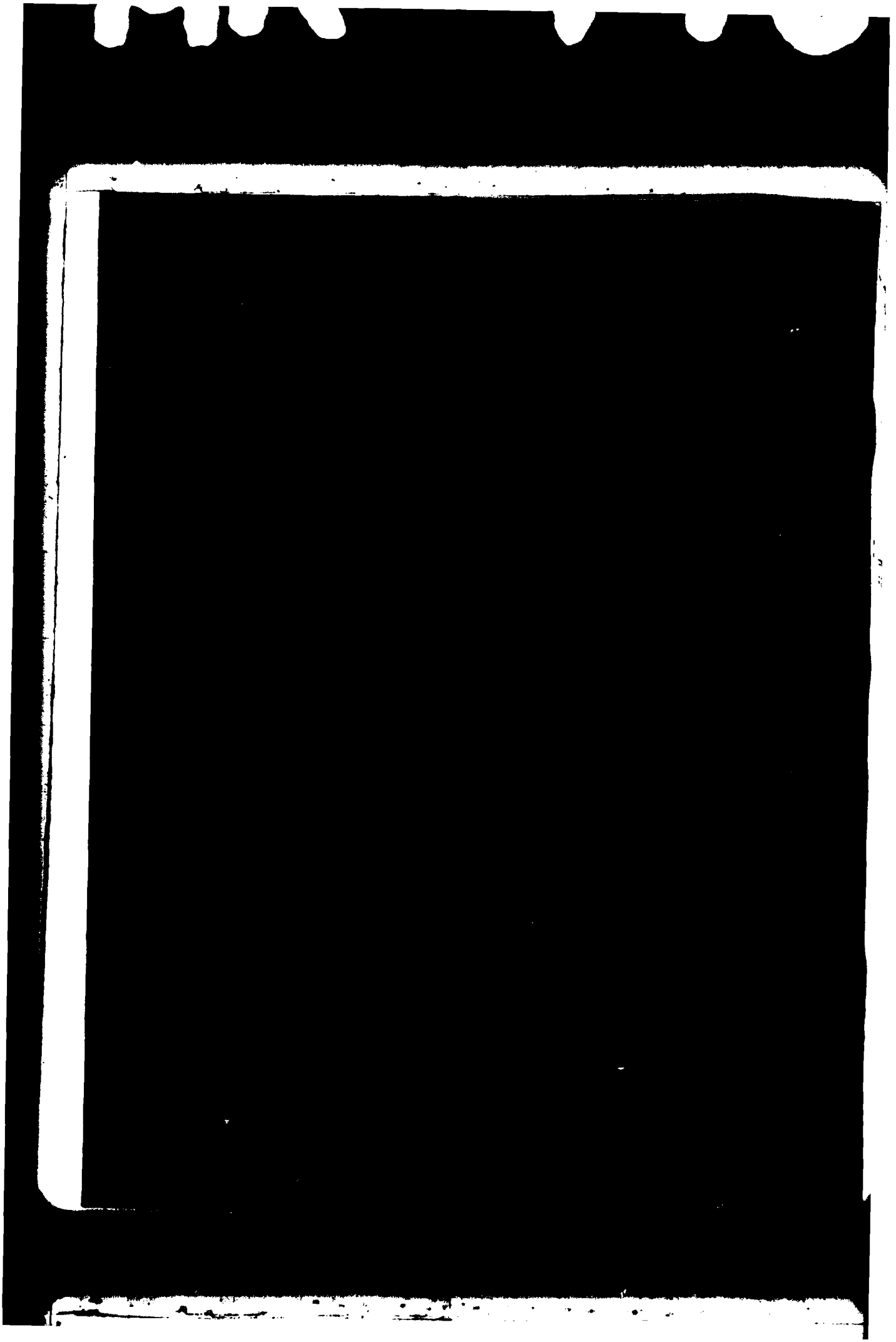

(14) NRL-MR-4405

SECURITY CLASSIFICATION OF THIS PAGE (When Data Entered)

(9) REPORT DOCUMENTATION PAGE

READ INSTRUCTIONS BEFORE COMPLETING FORM

1. REPORT NUMBER	2. GOVT ACCESSION NO.	3. RECIPIENT'S CATALOG NUMBER
NRL Memorandum Report 4405	AD-A098	896

4. TITLE (and Subtitle)

(6) AN INITIAL STUDY OF THE INJECTION OF AN INTENSE RELATIVISTIC ELECTRON BEAM INTO THE ATMOSPHERE

5. TYPE OF REPORT & PERIOD COVERED
Interim report on a continuing NRL problem.

6. PERFORMING ORG. REPORT NUMBER

7. AUTHOR(s)

(10) R. B. Fiorito*, R. F. Fernsler†, J. R. Greig, M. Herndon, I. M. Vitkovitsky, A. W. Ali and V. E. Scherrer

8. CONTRACT OR GRANT NUMBER(s)

(11) 4 Mar 81

9. PERFORMING ORGANIZATION NAME AND ADDRESS
Naval Research Laboratory
Washington, D.C. 20375

(16) R011-09

10. PROGRAM ELEMENT, PROJECT, TASK AREA & WORK UNIT NUMBERS
61153N; R011-09-41; 47-0871-0-0 and 61101E; 0; OR40AA

11. CONTROLLING OFFICE NAME AND ADDRESS
Office of Naval Research, Arlington, VA 22217
Defense Advanced Research Projects Agency, Arlington, VA 22209
ATTN: Program Management/MIS

12. REPORT DATE
March 4, 1981

13. NUMBER OF PAGES
52

(12) 49

14. MONITORING AGENCY NAME & ADDRESS (if different from Controlling Office)
Naval Surface Weapons Center
White Oak, MD 20910
ATTN: Code R401

(17) RR011-09-41

15. SECURITY CLASS. (of this report)

15a. DECLASSIFICATION/DOWNGRADING SCHEDULE

16. DISTRIBUTION STATEMENT (of this Report)
Approved for public release; distribution unlimited.

17. DISTRIBUTION STATEMENT (of the abstract entered in Block 20, if different from Report)

18. SUPPLEMENTARY NOTES
Research supported by the Office of Naval Research and by the Defense Advanced Research Projects Agency (DOD) ARPA Order No. 3718, monitored by the Naval Surface Weapons Center under Contract N60921-80-WR-W0189.
*Permanent address: Naval Surface Weapons Center, White Oak, MD 20910
†Permanent address: JAYCOR, Alexandria, VA 22304

19. KEY WORDS (Continue on reverse side if necessary and identify by block number)
Intense Relativistic Electron Beams
Charged Particle Beam
Atmosphere

20. ABSTRACT (Continue on reverse side if necessary and identify by block number)

Using the VEBA pulse generator (≲2 MV, ~60 kAmp, ~60 ns) and a field-emission diode with a titanium foil anode (≲43 μm), relativistic electron beams with $v/\gamma \gtrsim 0.5$ have been produced and injected into the atmosphere. Typical injected net currents were ~35 kAmps and there was little plasma return current (≲20%). These beams were observed to expand and contract at the betatron wavelength ($\lambda_\beta \gtrsim 12$ cm) as they propagated through the atmosphere and to become unstable at ~$3\lambda_\beta$. Observations were made in both visible light (2000-6000 Å) and x-radiation (10-100 keV). Peak current densities reached ~3kAmp/cm^2 at ~20 cm from the diode where the beam appeared to consist of two separate coaxial components both of near uniform current density. The central

(Continued)

DD FORM 1 JAN 73 1473 EDITION OF 1 NOV 65 IS OBSOLETE
S/N 0102-LF-014-6601

251950 slr

SECURITY CLASSIFICATION OF THIS PAGE (When Data Entered)

20. ABSTRACT (Continued)

component contained ~65% of the total beam current and was initially within a radius of ~1.4 cm. The outer component of the beam started with a radius of ~5 cm (defined by the anode foil) and appeared to expand steadily. The visible emissions belonged to the species N_2^+ and N_2 and were synchronous with the electron beam current. The absolute emission in the band $N_2^+1N(0\text{-}0)$ agreed with the calculated fluorescence intensity within experimental uncertainty, but the emission in the band $N_2 2P(0\text{-}0)$ was ~6 times larger than suggested by simple fluorescence calculations.

A simple technique was devised to select a fraction of the electron beam emerging from the diode to produce a pinched matched beam.

CONTENTS

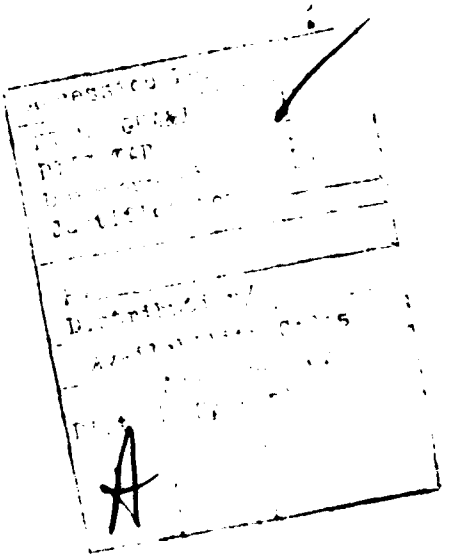

AN INITIAL STUDY OF THE INJECTION OF AN INTENSE RELATIVISTIC ELECTRON BEAM INTO THE ATMOSPHERE

I. INTRODUCTION

The interaction of intense relativistic electron beams (REBs) with gases has been the subject of numerous theoretical and experimental studies.[1-6] Most of these efforts have concerned gases at pressures considerably below atmospheric. The applications of such work include plasma heating,[6,7] collective ion acceleration[8] and the study of instabilities of REBs[1] as they propagate through gaseous media.

Relatively few experiments have been done at pressures near atmospheric even though such studies have application in a number of important areas of research including electron beam sustained lasers,[9] inertial confinement fusion[10] and particle beam weapons.[11] This has occurred partially because the analysis and diagnosis of intense beams interacting with high pressure gases are complex and difficult.

We have performed experiments which examine the interaction of an intense REB with air at atmospheric pressure.[12] A typical beam with net current ~35 kAmp and energy ~2 MV, propagated through the atmosphere showing marked betatron oscillations and becoming unstable within a few betatron wavelengths.[1,2] However, within this distance measurements were made of the x-ray Bremsstrahlung from the beam electrons, of the induced visible emissions from the air molecules, and of the beam current distribution. By selecting a fraction of the total beam current (~ 10%) using a carbon aperture, a pinched-matched beam[13] was produced. This beam propagated stably in the atmosphere showing only Nordsieck expansion.[14]

Manuscript submitted December 18, 1980.

II. APPARATUS

II-i. The VEBA Generator and Diode Assembly.

The relativistic electron beam was produced using the NRL VEBA (Versatile Electron Beam Accelerator)[15] with the pulse generator operated in the short pulse (FWHM~60 ns) mode. The accelerator consists of a 1.9 MV Marx generator, water Blumlein, and a tapered transmission line (20 Ω output impedance). The transmission line was terminated with a cold cathode diode as illustrated in Fig. 1. Depending on the matching of the diode to the transmission line impedance, the peak voltage appearing across the diode varied from ~0.75 to ~3 MV with the current in the diode varying correspondingly. The optimum diode configuration (Fig. 1) consisted of an annular brass cathode with outside diameter 20 mm and a titanium foil anode. The anodes used were annealed foils of thicknesses 1, 1.7, and 3 mils. The foils were attached to the end of VEBA with a vacuum-flange foil stretcher and had an exposed diameter of 10 cm. With the diode evacuated the foils bowed inward approximately 5 mm leaving an anode-cathode gap of 15 mm.

To achieve reproducible operation of the diode at ~40 Ω impedance i.e. in the cold cathode mode and to ensure significant electron beam extraction from the diode it was necessary to use a 28 mm lucite prepulse suppression switch in series with the diode (Fig. 1) and to operate at base pressures $\lesssim 3 \times 10^{-5}$ Torr. In addition the cathode had to be cleaned and sprayed with Aerodag graphite every few shots. The annular cathode allowed much higher currents than a hemispherical cathode of the same outside diameter. If there were sharp edges on the cathode, if the prepulse suppressor failed (usually for want of cleaning), or if the gas pressure was too high, premature plasma production in the diode allowed very high diode currents, very poor beam extraction through the anode foil, and usually ignited the anode foil (Fig. 2).

On all diode shots the voltage (V_D) appearing across the diode was recorded with a resistive divider on the cathode stalk, and the current in the diode (I_D) was recorded with a $\dot{B}$ probe placed in the side wall of the diode chamber (Fig. 3). A second resistive divider was used to measure the voltage on the Marx generator.

II-ii. Electron Beam Injection Configurations

The intense relativistic electron beam (REB) emerging through the titanium, anode foil was studied in three separate "air-side" configurations:

(1) The REB was stopped after propagating 20 cm through the air by a Faraday cup (Fig. 3). A current return path was provided in the form of a coaxial copper screen with diameter 15 cm. Without the low inductance current return path the Faraday cup (or any other "probe" placed in the beam) can reach very high voltages, sometimes sufficient to cause air breakdown (Fig. 4), and the would-be measurements become meaningless.

(2) To approximate "freely" propagating electron beams, the REB was injected into the open laboratory or into a large box (width $\sim$60 cm, height $\sim$150 cm, and length $\sim$200 cm) that was covered with copper screen and grounded to the VEBA generator around the anode assembly.

(3) By placing a carbon block, $\sim$1 cm thick by 11 cm diameter with a 1 cm diameter hole at its center, directly in front of the anode foil stretcher and grounding the block coaxially to the foil stretcher, most of the REB was stopped in the carbon block. The fraction of the beam that emerged through the hole in the carbon block was dependent on the separation of the block from the anode foil. When this distance was set at $\sim$4 cm, $\sim$10% of the total beam current passed through the aperture in the carbon block.

In each of these configurations the net current in the REB was measured with Rogowski coils and/or the Faraday cup. The different devices were calibrated using the Faraday cup in the place of the anode foil, and short-circuiting the cathode directly to the collector of the Faraday cup. The Rogowski coils which are both 14 cm in diameter were placed around the cathode shank. In this situation the agreement between the four current monitors (the $\dot{B}$-loop measuring I_D, two Rogowski coils, and the Faraday cup) was within $\pm$5%.

III. RESULTS AND ANALYSIS

III-i. Measurement of the Current Distribution at the Anode Foil

Because of the difficulty of making measurements inside these high voltage diodes only a crude estimate of the current distribution was obtained. The low background gas pressure ($\lesssim 3 \times 10^{-5}$ Torr) inside the diode and the effectiveness of the prepulse suppressor ensured that the current initially measured by the $\dot{B}$ probe inside the diode (I_D) was essentially all beam current, i.e., there was negligible plasma current inside the diode. However, all the current leaving the cathode does not necessarily pass through the anode foil. To measure the beam current passing through the 10 cm diameter aperture of the anode foil a Rogowski coil was placed against the foil stretcher (position 1 in Fig. 3) as described in § III-ii. In that configuration, the Rogowski coil measured the same current as the diode monitor, $I_{RC1} \sim I_D$, for $t \lesssim 70$ ns, indicating that all the diode current passed through the anode foil.

Next, the Faraday cup was connected directly to VEBA so that the cup's carbon collecting block became the anode of the diode. [This was the same position as for calibrating the Faraday cup except that the diode was not shorted.] With the same anode-cathode gap the average current ratio $\frac{I_{FC}(\text{peak})}{I_D(\text{peak})}$ was 0.65 ± 0.05. The diameter of the carbon collecting block in the Faraday cup was 8.9 cm, thus if the current density at the anode foil were uniform over the 10 cm foil diameter, the fraction of the current collected by the Faraday cup would be

$$\frac{I_{FC}(\text{peak})}{I_D(\text{peak})} \sim 0.8.$$

This suggests that ~35% of the current flowed in an annulus of radius $4.5 < r < 5$ cm.

From a comparison of Figs. 5 and 7, it is clear that using the Faraday cup in place of the titanium anode foil caused larger currents to flow in the diode and held down the diode voltage towards the end of the pulse. This may have been due to a small decrease in the anode-cathode gap or to the difference between titanium and carbon as anode materials. [The collector of the Faraday cup was a block of graphitic carbon.]

Some time integrated evidence suggests that the current flowing through the central region of the anode foil is pinched. For instance on many shots damage to the anode foil consisted of a small hole (~3 mm diameter) approximately in the center of the foil. Yet the time averaged beam current propagating through the anode foil is clearly not pinched at the foil but pinches ~3 cm outside the anode foil (see Figs. 6 and 10). [In all cases the loss of beam current due to scattering in the foil was negligible.]

From this fragmentary evidence of what is happening inside the diode we can only conclude that the current distribution at the anode foil is not uniform nor approximately a Bennett distribution, but rather there is a substantial current (~35%) flowing in an outer annulus ($r \sim 4.5$ cm) and of the remaining current (~65%) the current density probably peaks on axis though the beam is not pinched at the anode foil.

III-ii. Electron Beam Propagation Inside a Conducting Tube

In an effort to measure the net current distribution within the range of pseudo-stable propagation (Fig. 10, $z \leqslant 30$ cm) the REB was intercepted after propagating a distance of 20 cm with a Faraday cup (§III-ii and Fig. 3). Typical current and voltage traces for propagation in the presence of the copper screen current return path are shown in Fig. 7. Clearly all three current monitors indicate currents that rise with the diode voltage and reach peak values simultaneously. However both the Faraday cup current, I_{FC}, and the Rogowski coil current, I_{RC1}, fall with the voltage while the diode current, I_D, persists. Since this current in the tail of I_D flows at very low diode impedance it must be plasma current inside the diode. At the same time, up to the peak of I_D the ratio

$$\frac{I_{RC1}}{I_D} \sim 1.00 \pm 0.05;$$

thus, as indicated in §III-i, I_{RC1} measures the beam current,

$$I_{RC1} \sim I_{Beam}.$$

Such a relationship means that the impedance of the return current path through the coaxial copper screen is small compared to the impedance of the current return path through the beam generated air-plasma.

Open shutter photographs (Fig. 6) taken in visible light show the REB collapsing and expanding as it propagates inside the return screen with approximately the same betatron wavelength as the freely propagating electron beam (§III.iii).

A series of carbon apertures was placed over the FC to measure the beam current density at position 2. The currents measured by the Rogowski coil and Faraday cup are shown in Fig. 8. The current pulse shortens with decreasing aperture diameter indicating that the REB either expands later in the current pulse or is deflected from the axis. A plot of the current density distributions for two different times, t = 70 ns (time of peak current) and t = 30 ns (time of peak current density), along with a Bennett distribution with radius a = 1.4 cm is given in Fig. 9. Clearly the distribution at position 2 is changing rapidly with time and is not a Bennett distribution. At the same time the current measured by the Faraday cup with the largest aperture (diameter ~8.9cm) was such that

$$I_{FC}(peak)/I_{RC1}(peak) \sim 0.5,$$

suggesting once again that a substantial fraction of the beam current flows in an annulus with radius $\geq$ 4.5 cm.

III-iii. Freely Propagating Electron Beams

Freely propagating electron beams were studied in the open laboratory or in a large box covered with copper screen (§II-ii). There was no obvious difference between these two situations as far as beam propagation and dynamics were concerned. However, the presence of the copper screen significantly reduced the electromagnetic pulse (EMP) generated by injecting the beam into the atmosphere. No attempt was made to characterize this EMP, but the following diagnostics were used to

examine the interaction of the beam with the atmosphere: visible and x-ray photography, time integrated and time resolved spectroscopy, thermoluminescent x-ray detectors (TLDs), and Schlieren photography.

The freely propagating electron beam produced a luminous region in the atmosphere which could be photographed (Fig. 10). The most intensely luminous region was contained within a radius of ~2 cm over an axial extent of 20 to 30 cm. But even within this axial distance, light was emitted out to radii of at least 7 cm. Beyond this axial range the beam appeared to become unstable and to be deflected in different directions. No attempt was made to maximize the stable propagation range since the purpose of the experiment—to diagnose the beam and air channel—was readily accomplished in the 20-30 cm range.

The x-ray photograph (Fig. 11) as well as the higher contrast black and white photographs show the same periodic structure seen in Figs. 6 and 10. Intense spots of visible and x-ray light occur a few centimeters beyond the anode and repeat every ~ 6 cm to a range of 15-20 cm in the axial direction. The x-ray photograph also shows that the most intense x-ray emission is confined to a diameter of a few centimeters in agreement with the visible light photographs.

Two Rogowski coils (§II-ii) were used to measure the net current at 1, 6.5 and 15 cm axial distance (z) from the anode foil. These coils indicated a ratio $I_{RC}(\text{peak})/I_D(\text{peak}) = 0.78 \pm 0.05$ for all distances. No significant differences were observed when either 0.0017" or 0.001" thick foils were used. Examples of the Rogowski coil currents at $z = 0$ and $z = 15$ cm are given in Fig. 12.

We note that for the freely propagating REB the net current measured by the two Rogowski coils no longer rises or falls with the diode voltage as it did in the presence of the copper screen (§II-ii). This difference we believe is due to plasma currents driven by the beam induced voltage, $L\frac{dI}{dt}$, where L is the inductance of the REB propagating in the atmosphere and I is the net current.

A Schlieren system illuminated by a Korad ruby laser (pulse length -25 ns) was set up to observe the expanding air channel formed by the passage of the freely propagating electron beam in the range $z = 3$-16 cm from the anode foil. [Part of the system and the beam path (enhanced for photographic purposes) are visible in Fig. 2.] Schlieren photographs of the channel were taken at 3, 8, 30 and 100 μs after passage of the REB. No sharp density gradients were visible which could be identified with the channel. (The minimum detectable gradient for the system is 10^{20} cm^{-3}/cm.) At 100 μs however, a shock front was seen propagating outward with an average velocity of $\leqslant 1.6 \times 10^4$ cm/sec. The lack of an observable density gradient produced by beam induced heating of the air indicates that the time averaged radial distribution of beam current density did not have a sharp gradient.

The emission from the electron beam heated air channel was recorded with a Spex 0.75 m spectrograph/monochromator. Time integrated visible spectra were obtained by the accumulation of light from four shots, since the output for one shot was too weak (Polaroid Film with ASA 3000 was used). The spectrograph slit was focused on a vertical cross-section of the channel 7.5 cm from the anode. Spectra were recorded in the wavelength range 2000 to 6000 Å. The observed spectrum with identification is shown in Fig. 13. No emissions were observed above 4400 Å, and only emissions from N_2 and N_2^+ were observed. The identified spectrum includes all the strong bands in the spectra of N_2 and N_2^+ in this region.[16]

Two of the observed bands, N_2 2 P (0—0) at $\lambda \sim 3371$ Å and N_2^+ 1 N (0—0) at $\lambda \sim 3914$ Å were time resolved using a 1P28 photomultiplier attached to the exit slit of the monochromator. For this measurement the photomultiplier had to be completely shielded in a 1 inch thick lead housing to stop the scattered x-radiation with additional lead shielding to stop the direct x-radiation. Light input to the photomultiplier was reflected from a small mirror inside the housing. Figure 14 shows a comparison of a typical diode current (I_D) and photomultiplier currents for (a) N_2 2P (0—0) and (b) N_2^+ 1N (0—0). The photomultiplier currents have a smoother and flatter time variation than I_D and cutoff following the diode voltage (dotted line on I_D trace). All currents reach their maximum value at about 50 ns.

To obtain absolute intensities of these two bands the monochromator/photomultiplier system was calibrated using a calibrated tungsten lamp.[17] The measured emitted powers per unit length of beam path in the atmosphere, P, were

$$P\{N_2\ 2P(0\text{–}0)\} \sim 10^4 \text{ watts/cm}$$

and

$$P\{N_2^+\ 1N(0\text{–}0)\} \sim 1.5 \times 10^3 \text{ watts/cm},$$

and the uncertainty on these numbers was $\times\ 2^{\pm 1}$.

Calibrated thermoluminescent chips ($\frac{1}{8} \times \frac{1}{8} \times \frac{1}{32}$ inches) of CaF_2 were used to measure the x-ray dose produced by the beam. The chips were placed directly within the pinhole of the x-ray pinhole camera approximately 75 cm from the REB axis. In this configuration the field of view along the beam axis was ~19 cm. The dose measured was ~25 mR and was well above the minimum detectable signal. Unfortunately no energy selecting filters were used with these detectors so that although they are linear devices[18] in the range 100 keV to 10 MeV, the large, non-linear response below 100 keV prevented the interpretation of this signal as energy deposited by the REB in the atmosphere.

III-iv. Selecting a Pinched-Matched Beam

Although the freely propagating beam described in §III-iii was adequate for the preliminary studies planned in these experiments it was clearly so unstable that it could not be used in some of the more detailed beam propagation experiments planned for the future. Therefore techniques were examined that would allow us to produce a pinched, matched beam[13] from the simple pulse generator/diode combination. This was achieved by placing a carbon aperture stop in front of the diode (§II-ii). Varying the distance between the carbon block and the anode foil adjusted the beam current coming through the 1 cm diameter hole in the carbon block. With the carbon block ~7 cm from the anode foil so much current came through the 1 cm aperture that the beam was still unstable. But with the carbon block ~4 cm from the anode foil $\lesssim$ 10% of the diode current came through the aperture and produced a pseudo-stable, pinched, matched beam (Fig. 15). After emerging from the aperture the beam

expanded rapidly to reach Bennett equilibrium at a diameter of 3-4 cm. Thereafter the beam propagated through the atmosphere showing Nordsieck-like expansion and reaching a diameter of ~12 cm at a range of ~90 cm.

Time integrated spectra of the pinched, matched beam were identical to that in Fig. 13.

The net current in the pinched, matched beam was measured with a Rogowski coil placed next to the carbon block. This current and the comparison diode voltage and current are shown in Fig. 16. We notice that the current pulse coming through the aperture in the carbon block is shorter than the diode current pulse as it was with the Faraday cup measurements in §III-ii.

IV. DISCUSSION

From the measurements of the current flowing when the REB was propagating inside a conducting tube (§III-ii) we conclude that the current in the REB, I_b, was equal to the current measured in the diode, I_D, up to the peak of the diode voltage, i.e. for about the first 70 nsec. Thereafter the current in the REB fell with the diode voltage as seen by the Rogowski coil. Thus we can approximate the beam current by three successive linear variations as shown in Fig. 17. Both at the anode foil (§III-i) and 20 cm from the anode (§III-ii) there appeared to be two separate components to the REB. A central component containing ~65% of the total current was seen expanding and contracting at its betatron wavelength of ~12 cm. Assuming a uniform current distribution and approximately constant voltage of 2 MV this corresponds to a beam radius of $r_b \sim 1$ cm which compares favorably to the measured radius of the central component, $r_b \sim 1.4$ cm, at a distance of 20 cm from the anode foil. The outer component of the beam current was injected into the atmosphere with an outer radius of ~5 cm, the radius of the anode foil. But this component saw the magnetic field from the total net current, I_N, with peak value ~35 kA. Therefore for it $\lambda_\beta \sim 50$ cm which was too long to be observed.

The fact that the central component of the REB was seen to oscillate at its betatron wavelength means that at injection the beam temperature ($kT \sim \frac{1}{2}mv_\perp^2$) was much less than the Bennett temperature[19] for the beam, T_B, where

$$kT_B \simeq \frac{I_N e\beta}{2c},$$

or

$$kT_B \sim 14\ I_N(\text{amps})\ \text{eV}.$$

But at injection the beam temperature is dominated by the effects of scattering in the anode foil[20] and

$$kT_{\text{foil}} \sim \frac{4\pi n_0 Z^2 e^4 t}{\gamma m \beta^2 c^2} \ln\left[\frac{192\,\gamma\beta}{Z^{1/3}}\right]$$

where t is the foil thickness in cm. For titanium $kT_{foil} \sim 9.3 \times 10^7 \frac{t\beta^2}{\gamma}$ eV and we see that even for the thickest foil used (3 mil) the beam temperature at injection was small compared to the Bennett temperature. Therefore, as noted (§III-iii), the different foil thicknesses that were used had no noticeable effect on the freely propagating electron beam. As the REB propagated through the atmosphere, scattering from air molecules increased the beam temperature, but to reach the Bennett temperature the beam would have to have propagated ~80 cm and this appears to have been prevented by the growth of instabilities. The apparent break-up of the freely propagating beam at a range of 2 to 3 λ_β is consistent with the predictions of Lee[2] for the growth of the resistive hose instability. However, such detailed interpretation of time integrated photographs may be erroneous.

To model the REB propagating freely through the atmosphere we use the simple circuit shown in Fig. 18. We represent the generator as a current source for the beam current I_b, the air plasma as a resistance R_c through which the return current I_ρ flows, and all other return current paths by the inductance L_w through which the rest of the return current I_w flows. Then the net current I_N which is given by

$$I_N = I_b - I_\rho,$$

is equal to the current in the inductance I_w. The resistance of the air plasma R_c was calculated using the air chemistry code, CHMAIR[21]: (Note that the circuit behaviour depends only on the resistance and inductance per unit path length, so the length of the plasma column is not important.) The inductance L_w was calculated using an average beam radius and a guessed return current radius. Fortunately the inductance is very insensitive to these radii except in the case of propagation inside the conducting

tube where experimentally $\omega L_w << R_c$ where $\omega \sim 4 \times 10^7$ sec^{-1}, is the characteristic frequency associated with the beam pulse. Taking the average radius of the central component of the beam current as $\sim$1 cm, and assuming that all current returns to the generator within an outer radius of 45 cm, which is governed by the copper screened enclosure, we calculate the net current, I_N, flowing along the beam path as shown in Fig. 17. Though the current calculated from the model does not show the detailed structure of the measured net current the general characteristics of a reduced rate of rise, delayed and reduced peak value, and a lengthened current pulse are all present. Much more detailed modeling[22] could be used but is not practicable with the limited data available. The air chemistry code CHMAIR was also used to follow the electron density along the beam axis, $n_e(t)$, the electron temperature, $T_e(t)$, and the gas kinetic temperature, $T_g(t)$. These are shown in Fig. 19. After 200 ns changes occur slowly; at 1 μs, $T_e \sim T_v \sim 0.32$ eV and $T_g \sim 0.1$ eV where T_v is the vibrational temperature of N_2. CHMAIR has no hydrodynamics which is a good approximation during the beam pulse, but for times greater than a few microseconds gas dynamic effects should be taken into account. No direct measurements of n_e or T_e were made but in as much as the circuit model predicted the net current within $\pm$30% over the total beam pulse the calculated values of n_e and T_e must be of similar accuracy since they were used to calculate R_c. Note that in Fig. 17, I_N was calculated with and without the complex molecular ion N_4^+ in the code but this species has little effect on the net current in the circuit.

Using a steady state relation and neglecting excitation and deexcitation caused by secondary electrons the population of any excited state molecule in the air plasma can be written as

$$n^*(t) = \frac{J(t)\,\eta}{q + A}$$

where $J(t)$ is the beam current density, η is the efficiency of excitation by beam electrons for a given upper state, and q and A are the quenching and the spontaneous decay rates for that excited state. Excitation efficiencies and quenching rates have been determined for a number of excited states that are pertinent to the calculation of the emission from air plasmas.[23] The intensity emitted in a given molecular band is then

$$S(t) = n^*(t)\; A\; h\nu$$

where ν is the emission frequency.

Integrating over the current distribution, the intensity emitted per unit length of beam path is

$$P(t) = I_b(t)\,\frac{\eta A h\nu}{q + A}.$$

For N_2 2P (0–0)

$$P_1(t) \sim 1.6 \times 10^{-5}\,\frac{dE}{dx}\,I_b(t) \quad \text{watts/cm}$$

and for N_2^+ 1N(0–0)

$$P_2(t) \sim 5.7 \times 10^{-6}\,\frac{dE}{dx}\,I_b(t) \quad \text{watts/cm}$$

where $I_b(t)$ is the beam current in amperes and dE/dx is rate of loss of energy for the beam electrons in eV/cm. These equations are consistent with the measurements of Davidson and O'Neil[24] and predict a ratio of intensities of these two bands of

$$\frac{P_1(t)}{P_2(t)} \sim 3.$$

At the maximum beam current of ~40 kA the predicted intensities for these two bands are

$$P_1(40) \sim 1.5 \times 10^3 \quad \text{watts/cm}$$

and

$$P_2(40) \sim 0.5 \times 10^3 \quad \text{watts/cm.}$$

Given that the measured intensities are only accurate to within a factor of ~2, the measured intensity of N_2^+ 1N (0–0) agrees with the calculated intensity within experimental error but the measured intensity of N_2 2P (0–0) is ~× 6 larger than the calculated value. In more accurate measurements using a Febetron electron beam source at ~600 kV, Hill[25] found that the intensity of N_2 2P (0–0) was ~× 3 higher than calculated and has postulated that this is caused by population of the $N_2(C)$-state through the formation of N_4^+ as

$$N_2^+ + 2N_2 \rightarrow N_4^+ + N_2$$

and

$$N_4^+ + e \rightarrow N_2 + N_2(C).$$

[We note that if all the N_4^+ recombined to form $N_2(C)$ states, the emitted power within the 2P (0–0) band would be approximately 100 times larger than estimated from efficiency calculations.] Within experimental accuracy, our measurements are consistent with Hill's findings. However there are a number of other factors that could influence the intensities emitted from the electron beam excited air plasma. First, the calculations above assumed that the air plasma was optically thin and this may not be true especially for N_2^+ 1N (0–0). Most of the intensity in the P-branch of this band comes in a narrow spike at λ 3914 Å and at this wavelength the plasma could be optically thick. Second, because of the very non-thermal excitation there is a strong possibility that population inversions will exist among the N_2 excited states. Particularly the higher intensity of 2P (0–0) is attributed by one of us (AWA) as due to stimulated emission and other mechanisms such as

$$N_2(A) + N_2(A) \rightarrow N_2 + N_2(C).$$

Both effects are difficult to estimate because of the uncertain current distribution, the unknown bandwidth of the emission, and the uncertainty in the excited state populations. However, we suspect that both are significant and the present agreement between measured and calculated emissions for N_2^+ 1N (0–0) may be coincidence. More detailed analysis of this problem will be forthcoming through quantitative experimental measurements of n_e and T_e, and through utilization of our multispecies emission code which accounts for the excited state generation by a detailed calculation of the secondary electron distribution.[26]

Although we were able to photograph the freely propagating electron beam in x-radiation and obtained a signal well above the noise level (× 10) on the unfiltered thermoluminescent detectors (§ III-iii), it seems doubtful that quantitative measurements can be made with the TLDs (see Appendix). If a filtered TLD looking at radiation above 100 keV were able to see the same 19 cm of the beam path, the estimated signal due to x-ray emission perpendicular to the beam would be only ~ 1/30 of the signal observed in §III-iii which would give a signal to noise ratio of ~1.

For REBs with little or no induced plasma return current, a pinched, matched beam readily forms if the REB is injected into the atmosphere at or just above the Bennett temperature.[3] Thus using the

1.7 mil titanium foil and injecting at a radius of 0.5 cm we have

$$kT_{foil} \sim 8 \times 10^4 \text{ eV}$$

and for a matched beam

$$I_N \sim 5.7 \text{ kA}.$$

Then

$$\lambda_\beta \sim 24\, r_b.$$

Since the betatron frequency

$$\omega_\beta = \frac{2\pi\beta c}{\lambda_\beta} \gtrsim \frac{\epsilon_\gamma}{kT_\beta},$$

where ϵ_γ is the energy loss rate due to gas scattering, the beam follows a Nordsieck-like expansion as it propagates through the atmosphere as observed in §III-iv.

V. CONCLUSIONS

This has been a preliminary experiment to study the injection of intense relativistic electron beams into the atmosphere. Using a simple cold-cathode diode, an REB with $\nu/\gamma \sim 0.5$ has been extracted and injected into the atmosphere. Although this beam was unstable, apparently to the resistive hose instability, observations were possible over a beam path length of almost 30 cm.

Approximately 65% of the beam current was contained within a radius $\lesssim 1.5$ cm to form a central component of the REB with peak current density of ~ 3 kA/cm^2. At injection the REB was cold and particle motion was dominated by the effect of the self magnetic field. Thus, coherent betatron oscillation was observed until phase mixing due to scattering destroyed the coherence. When the REB with net current ~ 35 kA propagated freely in the atmosphere, the return current flowing through the beam produced air plasma was $\sim 20\%$ of the beam current. Comparison of this measured current with that calculated using our air chemistry code and a simple circuit model for the propagating beam, showed good qualitative agreement.

The interaction of the REB with the air molecules in the atmosphere produced both visible light and x-radiation at sufficient intensities to allow photographic recording. The visible emissions belonged

to the spectra of N_2 and N_2^+ but it is not clear that the intensities emitted were controlled by simple beam induced fluorescence. Much more complicated phenomena, including cascading chemical reactions and superradiance, may have been occurring.

Finally a simple technique using a carbon aperture has been devised for selecting a fraction of the beam current that is more suitable for propagation studies.

VI. ACKNOWLEDGMENTS

The authors thank Dr. R.K. Parker for providing access to the VEBA generator and thus making this experiment possible. We also thank Drs. R.E. Pechacek and M. Lampe for numerous discussions which have aided in our understanding of the observed phenomena, Dr. F. Young for assistance with the x-ray photographic diagnostics, and Dr. S. Gorbics who provided assistance with the TLD measurements and a calibration system.

Appendix

BREMSSTRAHLUNG PRODUCTION BY AN REB IN THE ATMOSPHERE AND ITS DETECTION WITH A TLD.

To make measurements using the thermoluminescent detector (TLD) the TLD was placed in the "pinhole" of the x-ray pinhole camera on the inside of the camera. In this position the "pinhole," which was drilled in a block of lead ~2 inches thick, defined a field of view for the TLD which included ~19 inches of the path of the REB.

Given normal density air and the beam current profile, and using the differential radiation cross section from Jackson,[27] we can calculate the Bremsstrahlung radiation emitted per unit length of beam path as a function of the angle between the emitted photons and the beam, ϕ, and the beam energy, γ. For a relativistic electron beam the bremsstrahlung emission is peaked in the forward direction with the half angle for the emission pattern being given by

$$\phi_{1/2} \sim \frac{1}{\gamma}$$

and the ratio of emitted intensity in the forward direction ($\phi = 0$) to that in the perpendicular direction ($\phi = \pi/2$) being

$$\frac{I(\phi = 0)}{I(\phi = \pi/2)} \sim \gamma^4.$$

The energy incident on the TLD depends on ϕ, on the solid angle subtended by the TLD at the beam, $\Delta\Omega$, and on the transmission of the atmosphere, $\exp(-\mu_{air} r)$, where μ_{air} is the absorption coefficient and r is the distance from the TLD to the beam. The energy absorbed by the TLD varies as $\{1 - \exp(-\mu_{TLD} \cdot d)\}$ where μ_{TLD} is the absorption coefficient of the detector material and d is its thickness. Curves for these variations are shown in Fig. 20 for $r = 75$ cm and $d = 1/32$ inch. Convolution of the bremsstrahlung emission from the REB at $\phi = \pi/2$ with the air transmission curve and

the TLD absorption curve followed by integration over all x-ray energies and over the beam pulse would give the net signal anticipated from the TLD. Unfortunately this integration is not simple and depends critically on the air cut-off value at low x-ray energies (~ 10 keV). Therefore interpretation of the measured signal (~25 mR) in terms of the total beam flux ($\int I_b(t)\, dt$) is not possible. However for x-ray energies above 100 keV the TLD response is almost constant; then the convolution and integration are both feasible and insensitive to the cut-off value. Thus, signals measured on a TLD with a filter that absorbed all radiation with energy less than 100 keV would be interpretable. For the 35 kA, ~2 MV beam used in these experiments the signal anticipated on the TLD (100 keV $\leqslant$ E_{photon} $\leqslant$ 1 MeV) would be ~0.78 mR and this would be less than the typical background signal (~1 to 2 mR).

VIII. REFERENCES

1. E.J. Lauer, R.J. Briggs, T.J. Fessenden, R.E. Hester, and E.P. Lee, Phys. Fluids, 21 1344-52 (1978).

2. E.P. Lee, Phys. Fluids, 21 1327-43 (1978).

3. R.J. Briggs, R.E. Hester, E.J. Lauer, E.P. Lee, and R.L. Spoerlein, Phys. Fluids, 19, 1007 (1976).

4. G. Wallis, K. Sauer, D. Sünder, S.E. Rosinskii, A.A. Rukhadze, and V.G. Rukhlin, Soviet Physics Usp. 17, 492 (1975) [review article].

5. A. Luches, V. Nassisi, and A. Perone, J. Appl. Phys. 50, 2505 (1979).

6. L. Thode, Phys. Fluids 19, 831 (1976).

7. D. Hammer, K.A. Gerber, and A.W. Ali, IEEE Trans. Plasma Science, PS-7, 83 (1979).

8. C. Olson and U. Schumaker, "Collective Ion Acceleration" Springer-Verlag, Berlin, 1979.

9. See for example, Ch. A. Brau, in "Excimer Lasers" edtd by C.K. Rhodes, Springer-Verlag, Berlin, 1979.

10. G. Yonas, Sci. Amer. **239**, 50 (1978).

11. J. Parmentola and K. Tsipis, Sci. Amer. **240** 54-65 (1979).

12. A.W. Ali, J.R. Greig, I.M. Vitkovitsky, R.B. Fiorito, and R.F. Fernsler, J. de Physique, Colloque 7, Supp. 7 July 1979 C7-773.

13. J.D. Lawson, "The Physics of Charged Particle Beams" (Clarendon, Oxford, 1977) p. 187, 195, and 211.

14. E.P. Lee, Physics of Fluids **19**, 160 (1976).

15. R.K. Parker and M. Ury NRL-MR 3056 (1975).

16. R.W. Pearse and A.G. Gaydon "The Identification of Molecular Spectra," 3rd Ed (Chapman and Hall, London, 1965) p. 209-220.

17. E.B. Turner in "Plasma Diagnostic Techniques" Edtd by R.H. Huddlestone and S.L. Leonard Academic Press, New York 1965 p. 319-358.

18. J.F. Fowler and F.H. Attix in "Radiation Dosimetry" 2nd ed. F.H. Attix and W.C. Roesch eds. Academic Press, New York, 1966. Vol. II p. 241.

19. L. Spitzer, "Physics of Fully Ionized Gases," 2nd Ed., Interscience New York, 1962 p. 109.

20. J.D. Jackson, "Classical Electrodynamics" Wiley, New York, 1962 p. 456.

21. R.F. Fernsler, A.W. Ali, J.R. Greig, and I.M. Vitkovitsky NRL-MR 4110 (1979).

22. D.A. McArthur and J.W. Poukey, Phys. of Fluids **16**, 1996-2004 (1973).

23. K.B. Mitchel, J. Chem. Phys. 53, 1795 (1970).

24. C. Davidson and R. O'Neil, J. Chem. Phys. 41, 3946-3955 (1964).

25. R.M. Hill (Stanford Research Institute, Menlo Park) private communication.

26. A.W. Ali and D. Strickland private communication.

27. J.D. Jackson "Classical Electrodynamics" (Wiley New York, 1962). 2nd ed. p. 715.

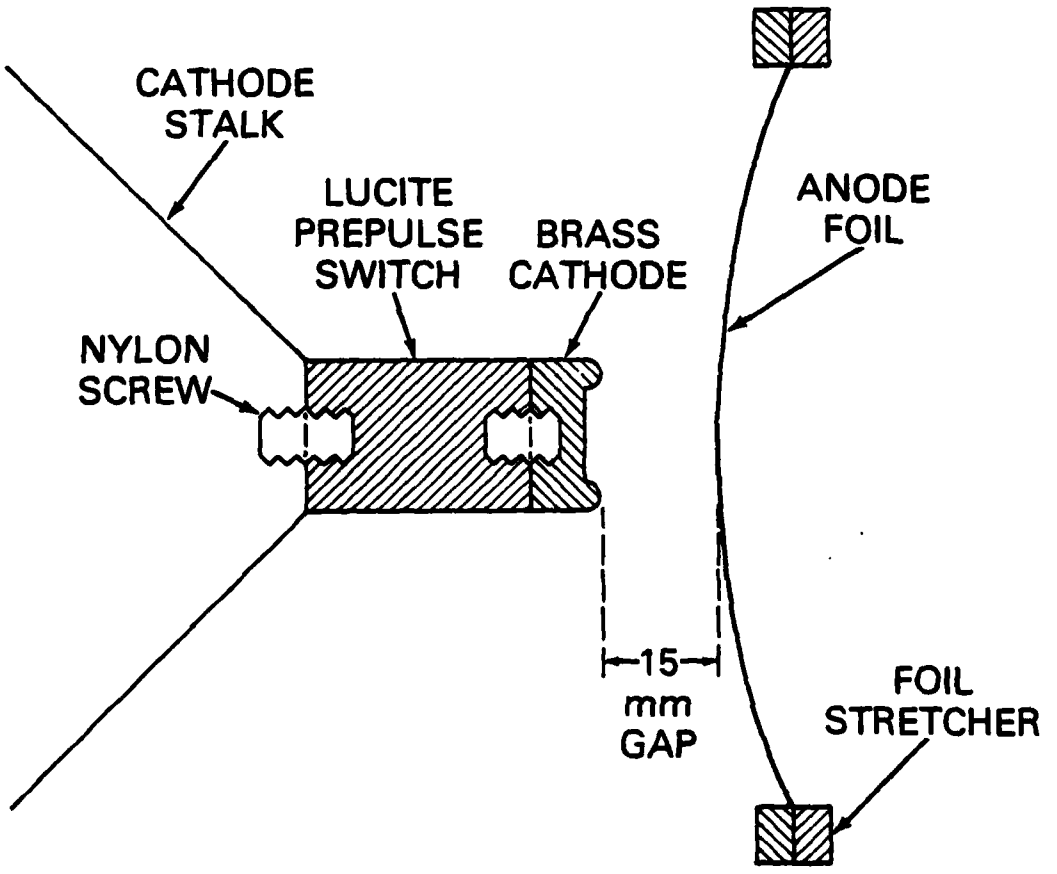

Figure 1 — The diode configuration

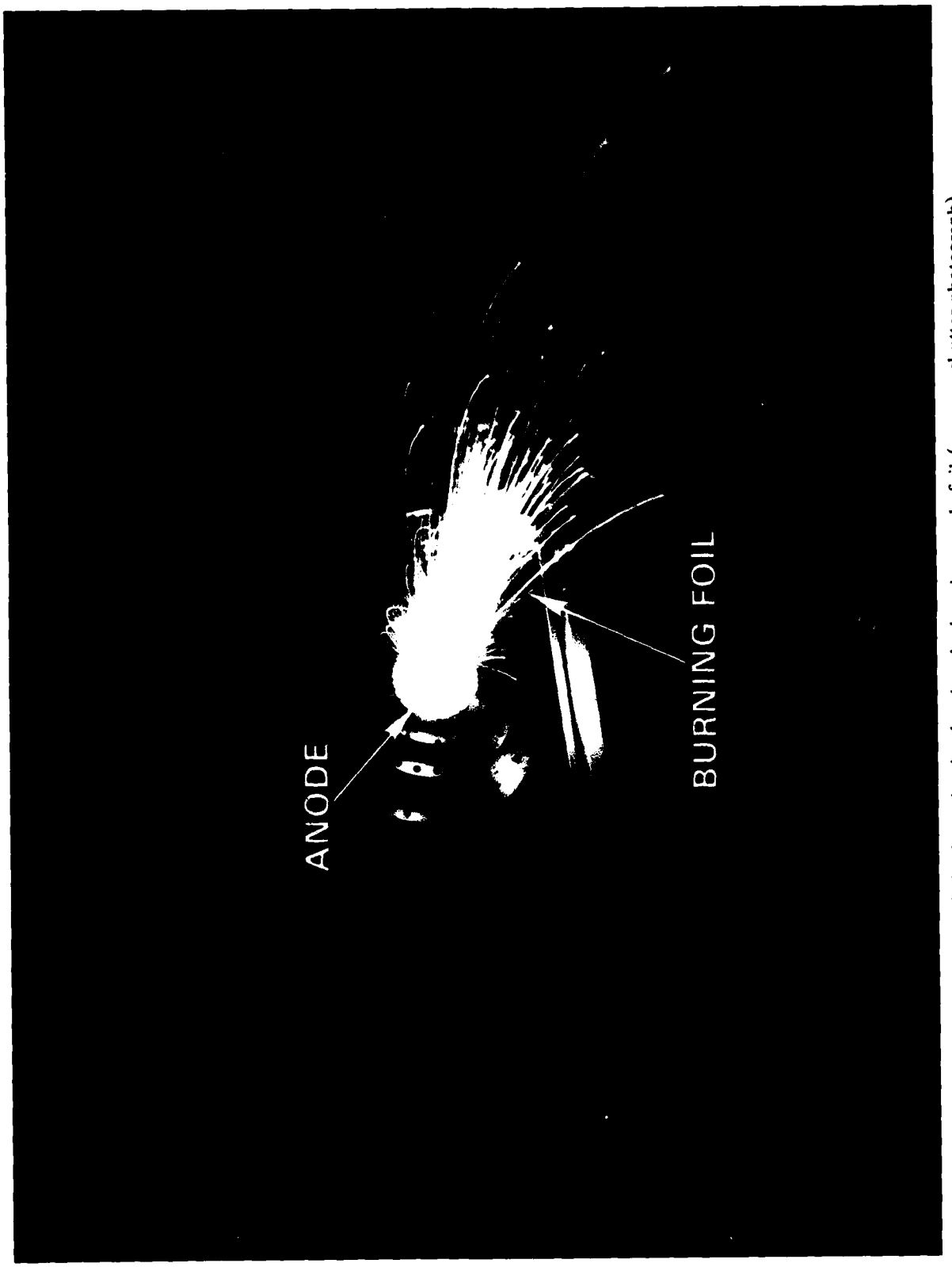

Figure 2 — A diode short circuit, showing the burning anode foil (an open shutter photograph).

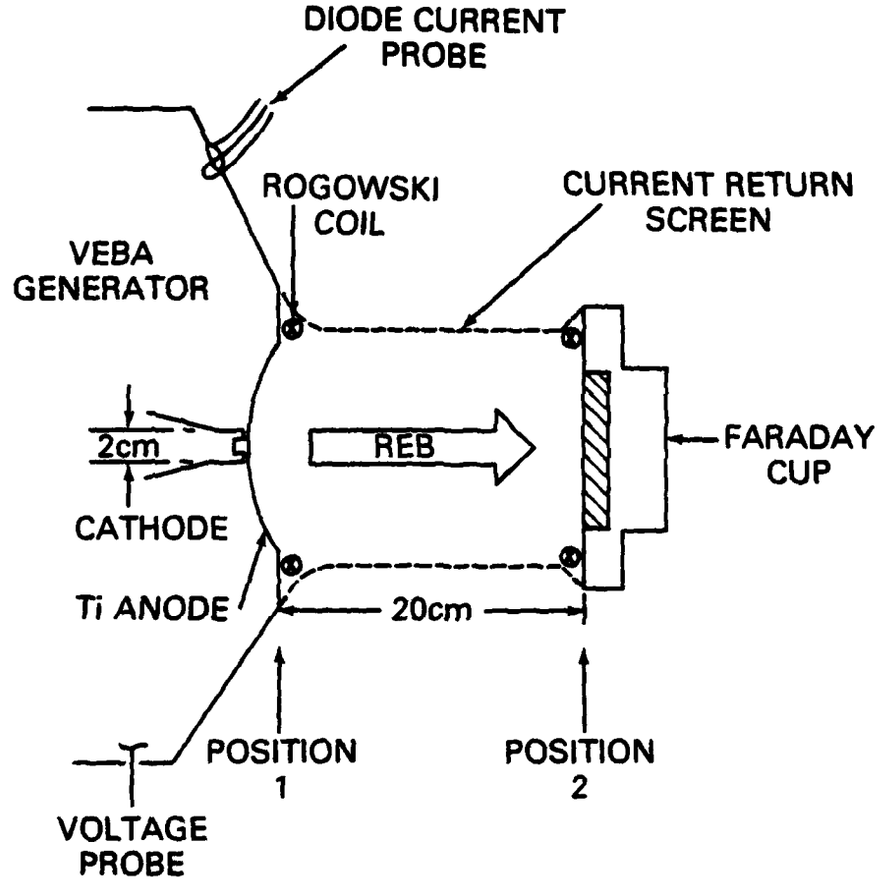

Figure 3 — Diode and beam diagnostics in the configuration using a current return screen.

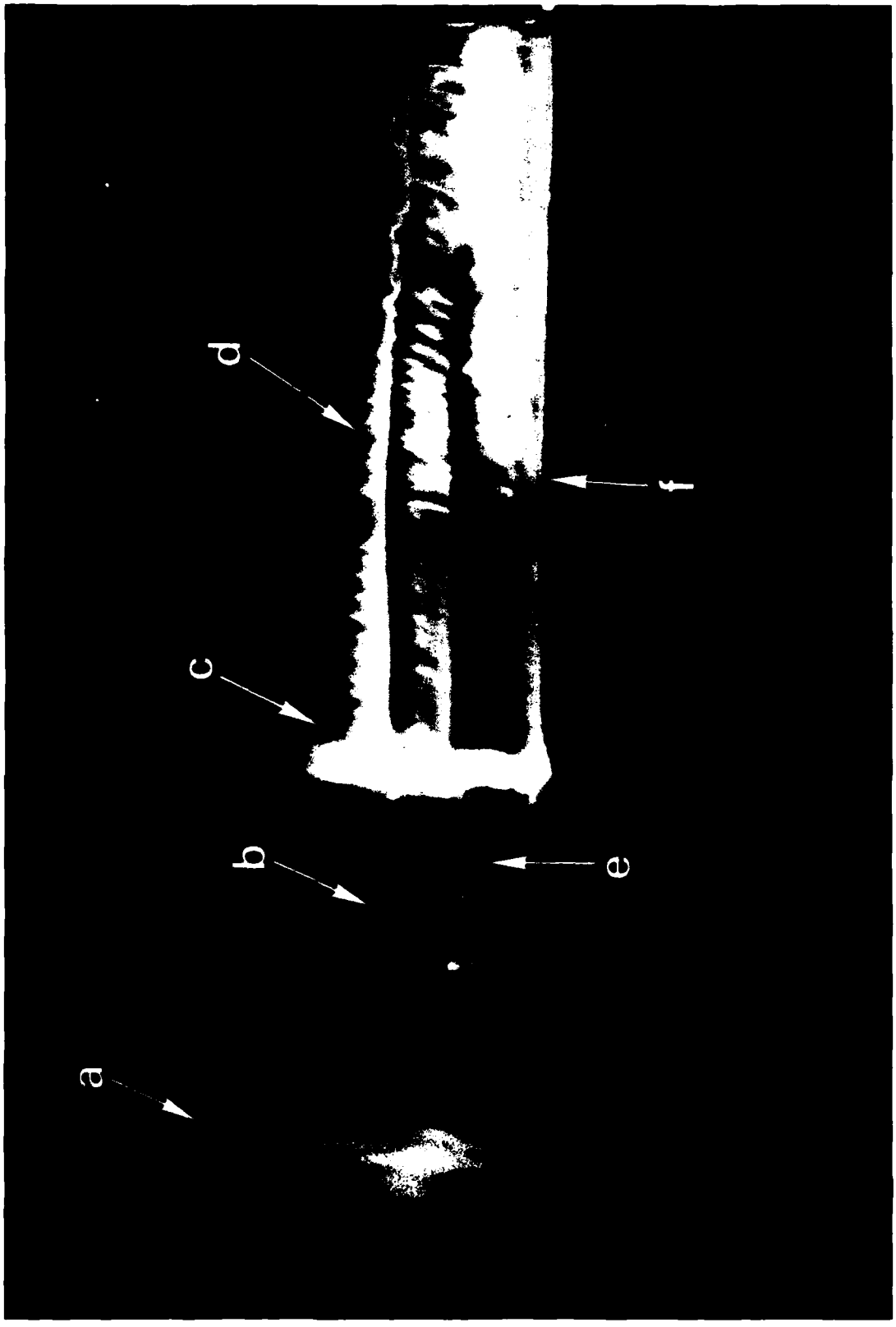

Figure 4 – Spurious effects generated when the electron beam is stopped by a poorly grounded Faraday cup. (a) The VEBA generator, (b) the anode foil, (c) the Faraday cup, (d) a coronal discharge (St. Elmo's Fire), (e) the electron beam (blue), and (f) the Faraday cup supports and cables.

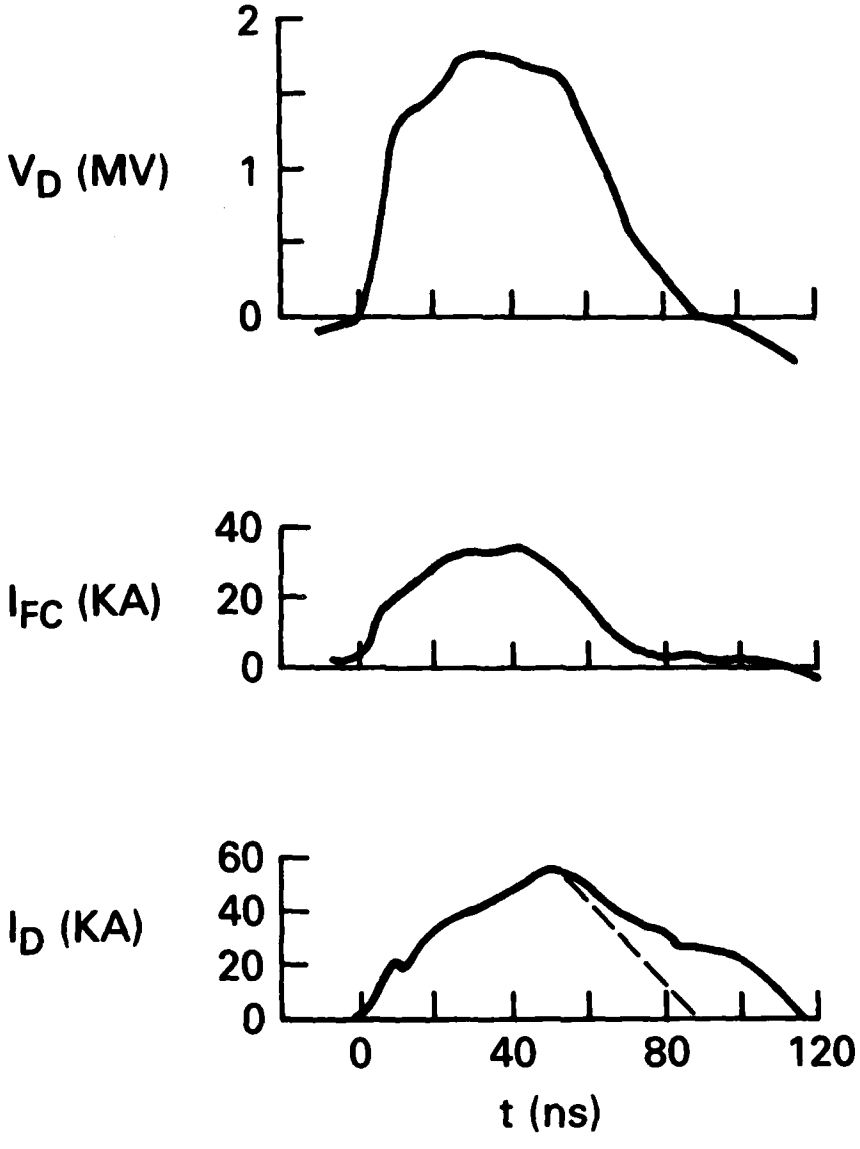

Figure 5 — Diode current and voltage characteristics with the Faraday cup as the anode. V_D is the diode voltage measured on the voltage monitor, I_{FC} is the current measured on the Faraday cup, and I_D is the current measured on the diode current monitor.

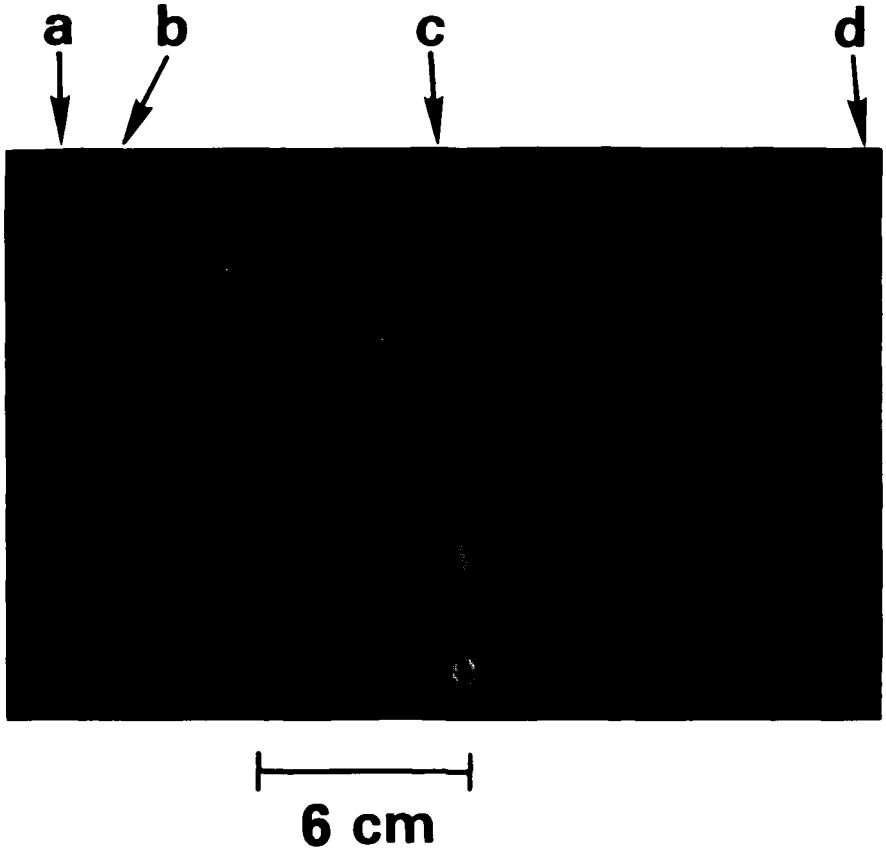

Figure 6 — An open shutter photograph of the electron beam propagating within the coaxial, current return screen. (a) is the anode foil, (b) is the Rogowski coil at position 1, (c) is the current return screen, (d) is the Faraday cup, and (e) is the electron beam showing betatron oscillations.

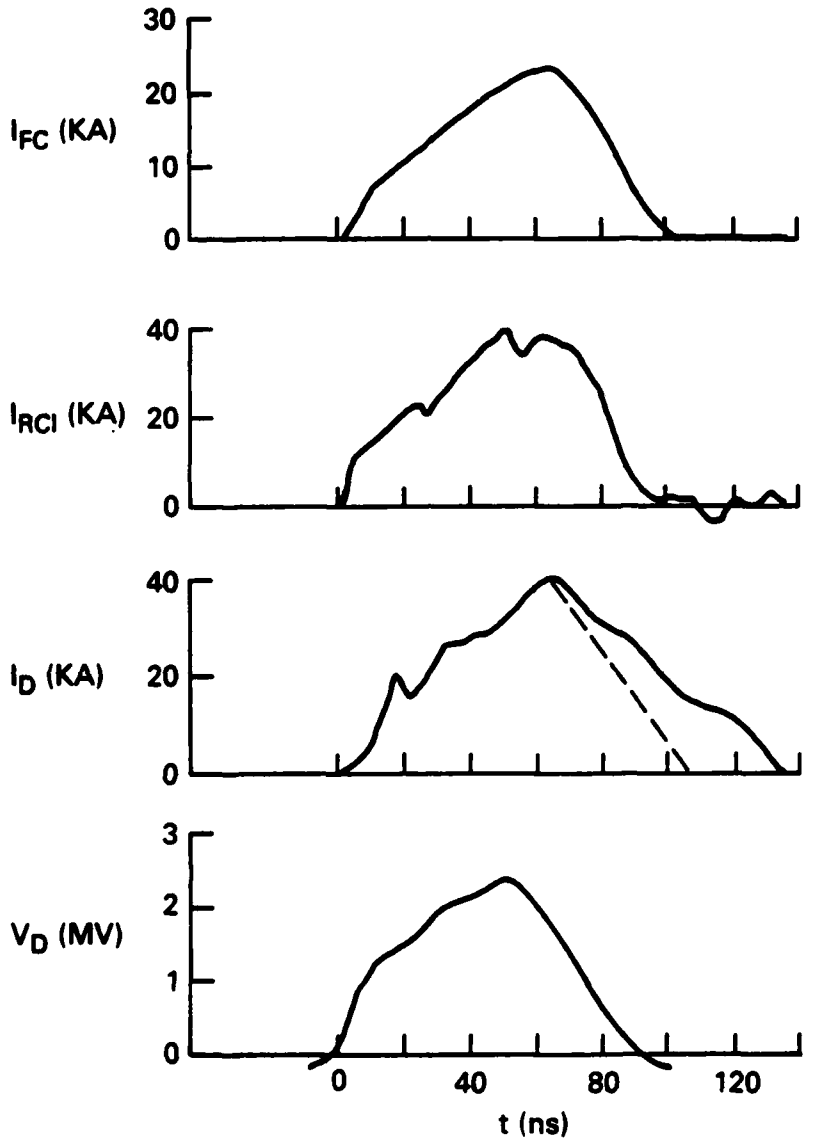

Figure 7 — Electrical parameters for an electron beam propagating within the coaxial current return screen. I_{FC} is the current measured on the Faraday cup, I_{RCI} is the current measured on the Rogowski coil at position 1, I_D is the current measured on the diode current monitor, and V_D is the voltage measured on the diode voltage monitor.

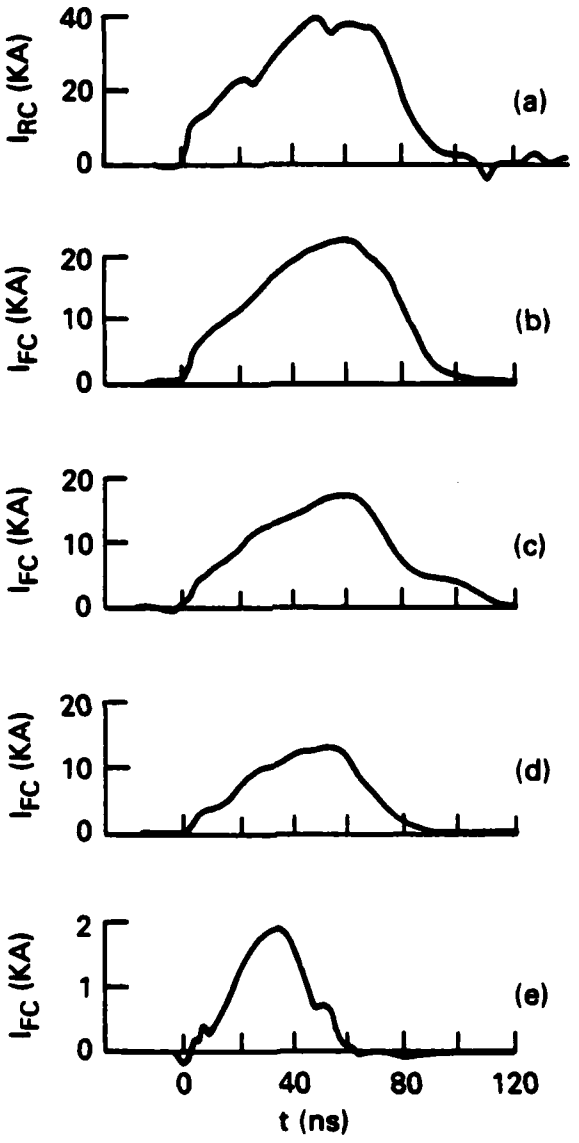

Figure 8 — Faraday cup current measurements for an electron beam propagating within the coaxial current return screen. Measurements are made with different carbon apertures in front of the Faraday cup to reduce its sensitive area. (a) is the current measured on the Rogowski coil at position 1 (coil diameter ~14 cm), (b), (c), (d), and (e) are the currents measured on the Faraday cup with apertures of 8.9 cm, 5.1 cm, 2.5 cm, and 1.0 cm respectively.

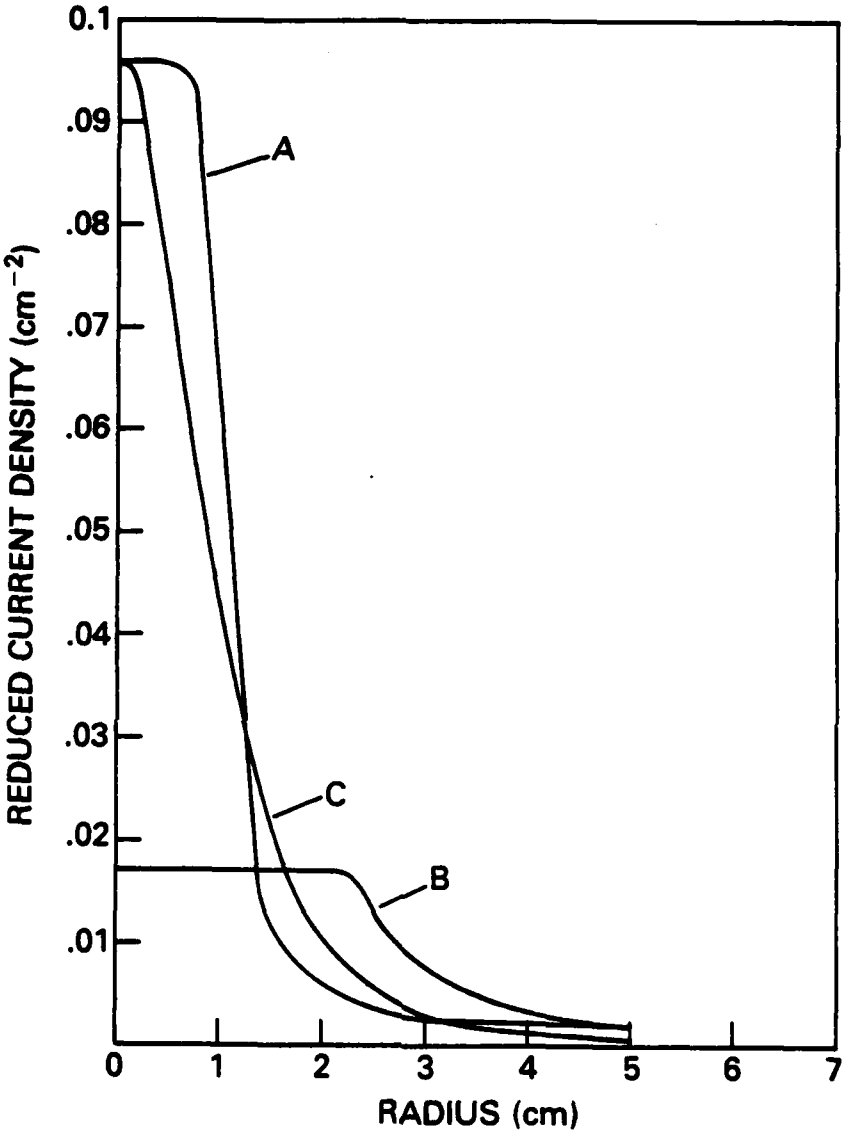

Figure 9 — Reduced current density distributions for an electron beam propagating within the coaxial current return screen. A is the measured distribution at t = 30 ns, B is the measured distribution at t = 70 ns, C is a Bennett distribution containing the same total current as A, the Bennett radius is 1.4 cm. The reduced current density is $J(r,t)/I(t)$ where $J(r,t)$ is the current density and $I(t)$ is the total current; $I(30)$ = 29 kA, and $I(70)$ = 36 kA.

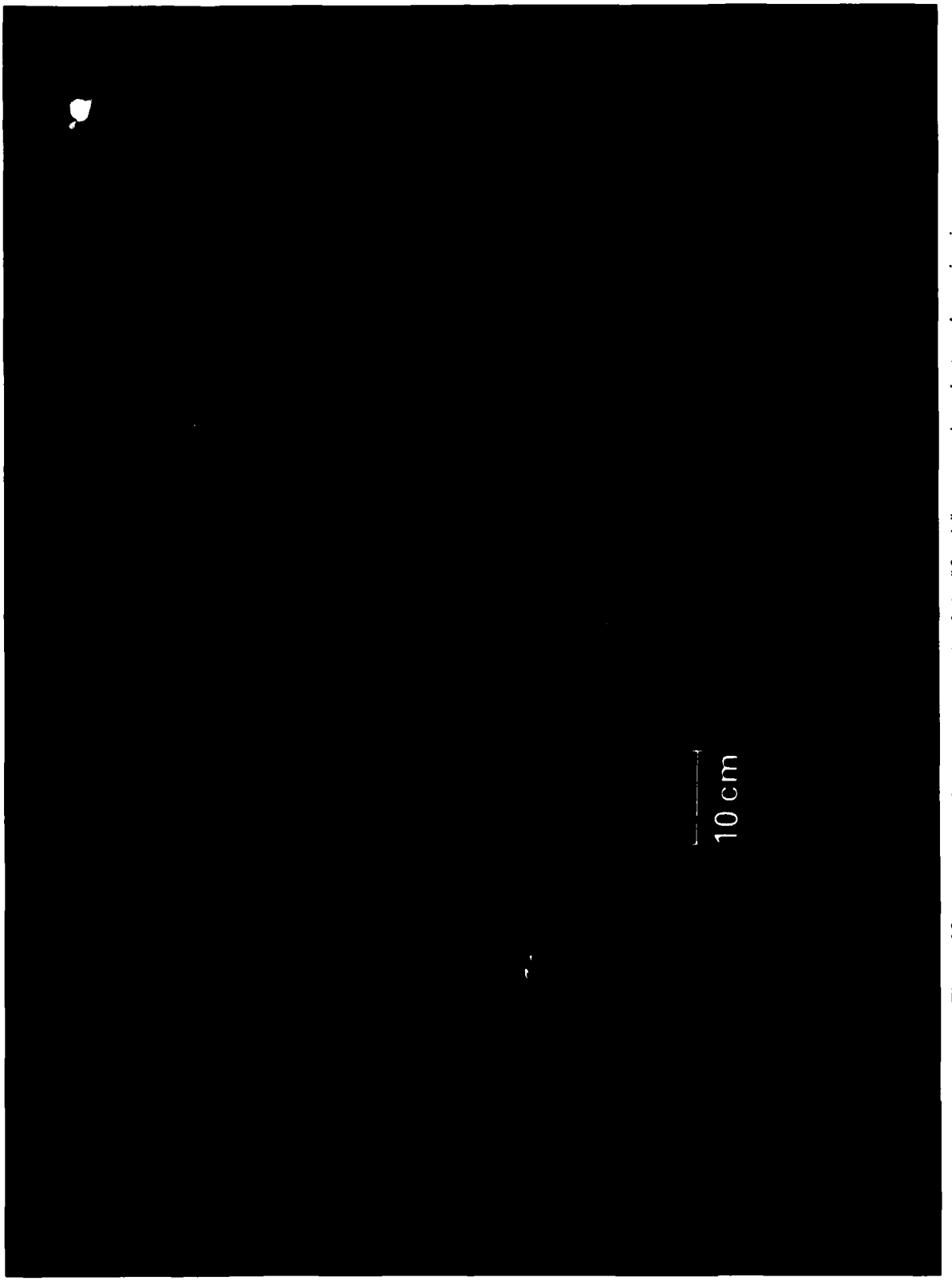

Figure 10 — An open shutter photograph of the "freely" propagating electron beam in air.

(Page 34 Blank)

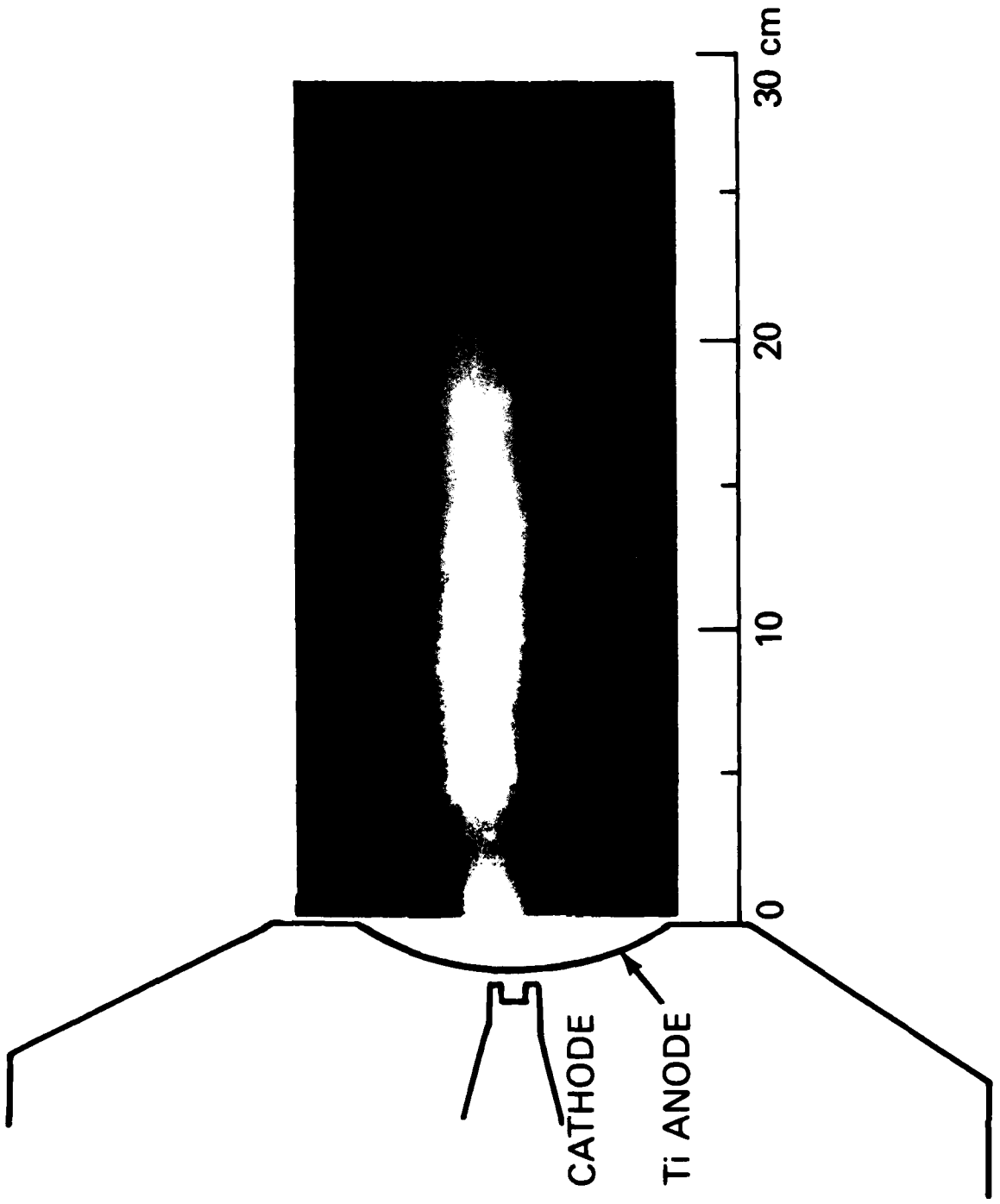

Figure 11 — An open shutter, x-ray pinhole camera photograph of the "freely" propagating electron in air (camera resolution ~0.5 cm).

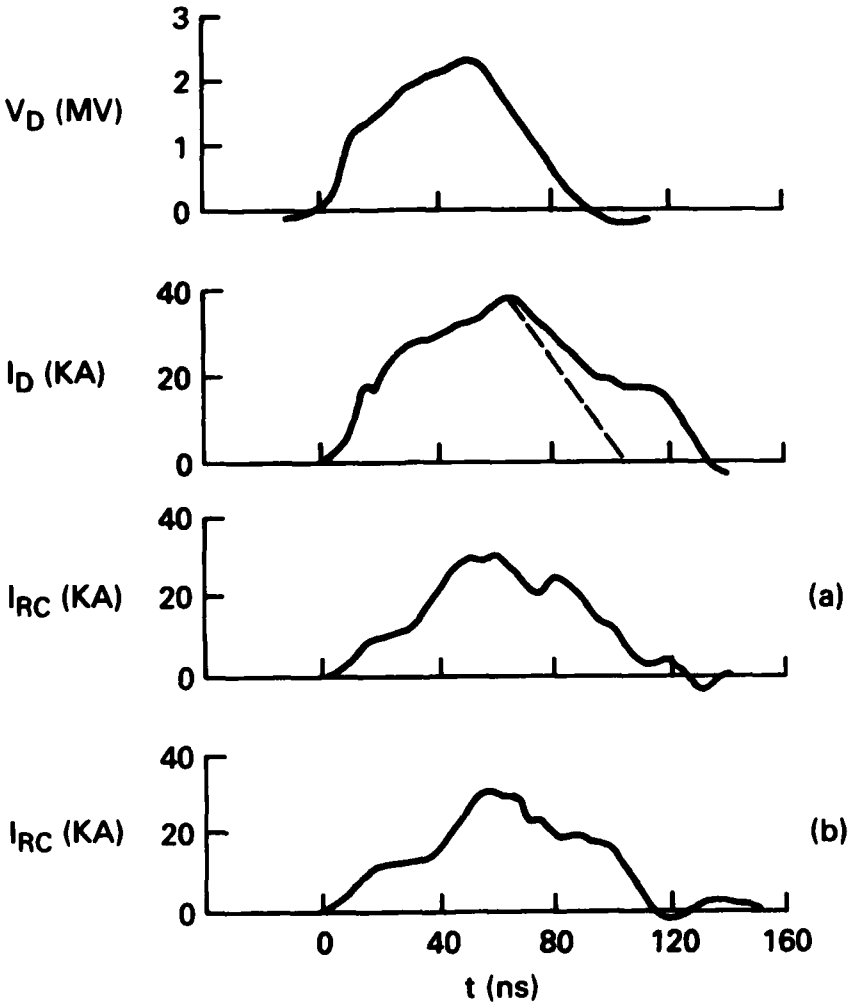

Figure 12 — Electrical parameters for the "freely" propagating electron beam in air. V_D is the voltage measured on the diode voltage monitor, I_D is the current measured on the diode current monitor, I_{RC} is the current measured on the Rogowski coil, (a) with the coil 15 cm from the anode foil, and (b) with the coil at the anode foil.

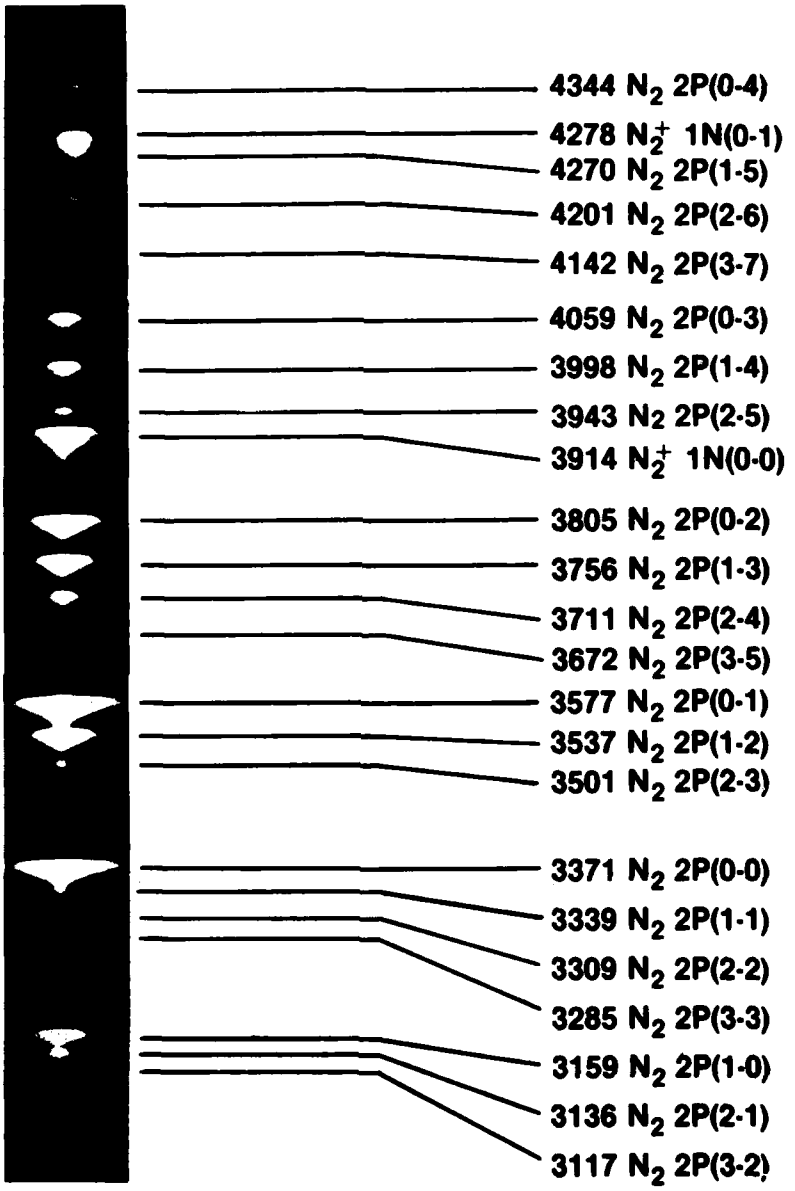

Figure 13 — The spectrum of the visible emissions from the intense electron beam propagating in the atmosphere. The wavelength resolution was 10 Å and the intensity distribution perpendicular to the wavelength axis represents the intensity distribution across a diameter of the electron beam ~7 cm from the anode foil with the total width of the photographic (black) image being 10 cm.

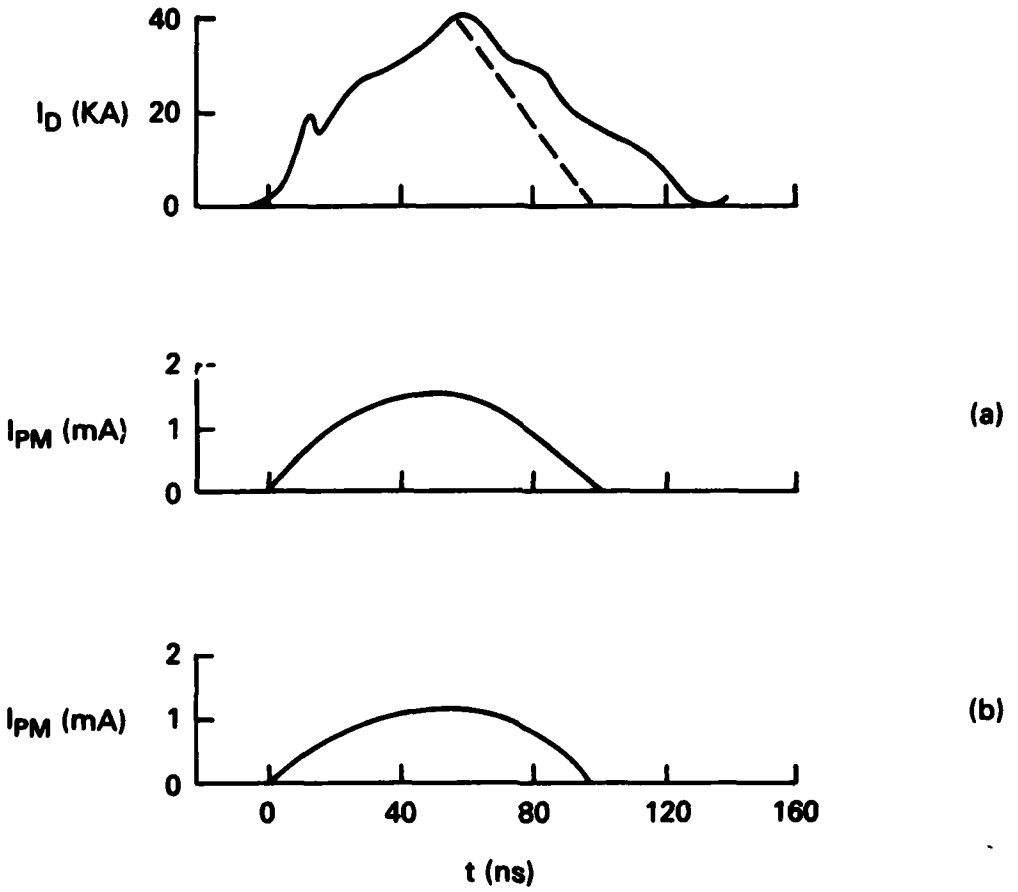

Figure 14 — The time dependence of the visible emissions from the intense electron beam propagating in the atmosphere. I_D is the current measured on the diode current monitor, I_{PM} is the measured photomultiplier current (a) at λ 3371 Å [$N_2 2P$ (0–0)], and (b) at λ 3914 A° [N_2^+ IN (0–0)]. The photomultiplier "saw" the whole beam diameter at ~3 cm from the anode foil.

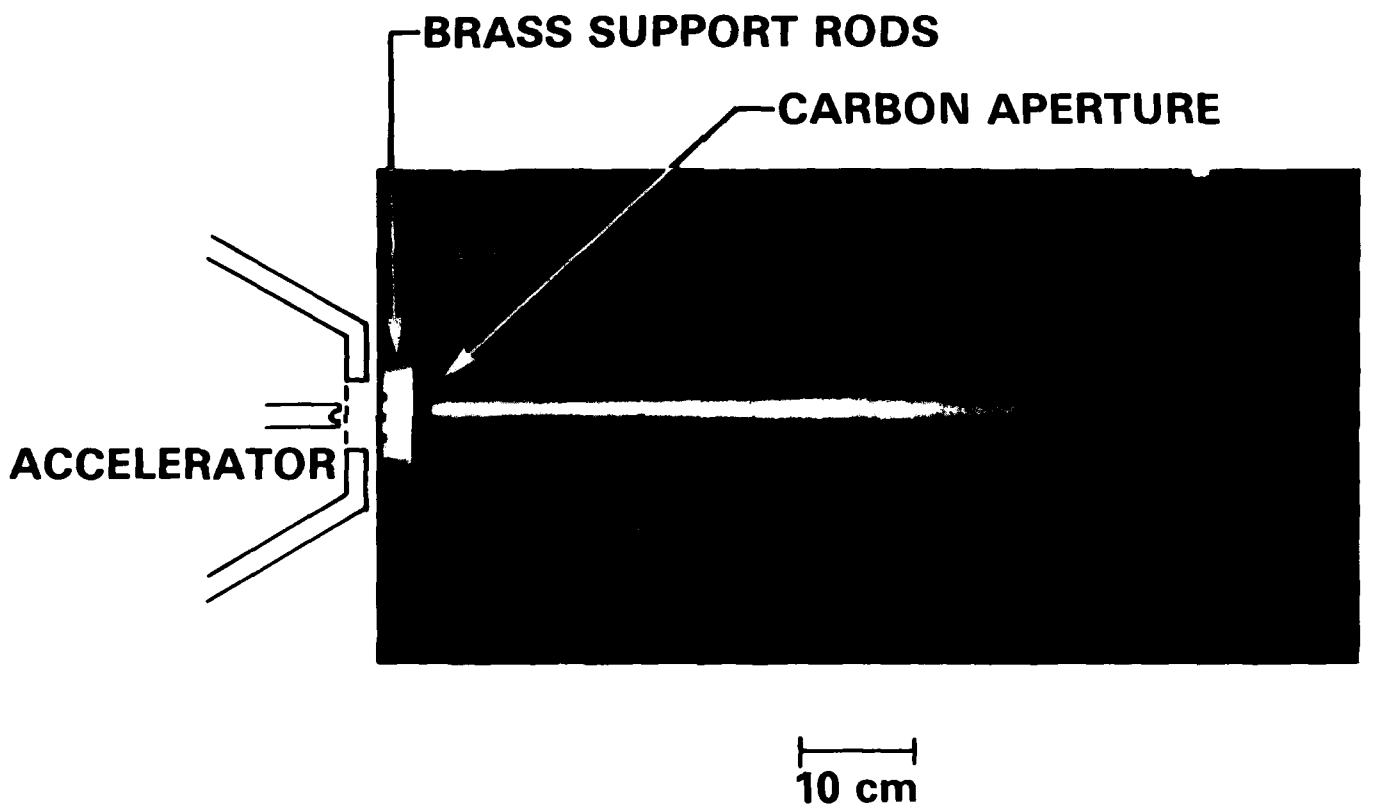

Figure 15 — An open shutter photograph of the electron beam passing through a 1 cm aperture and propagating "freely" in the atmosphere as a "pinched matched beam".

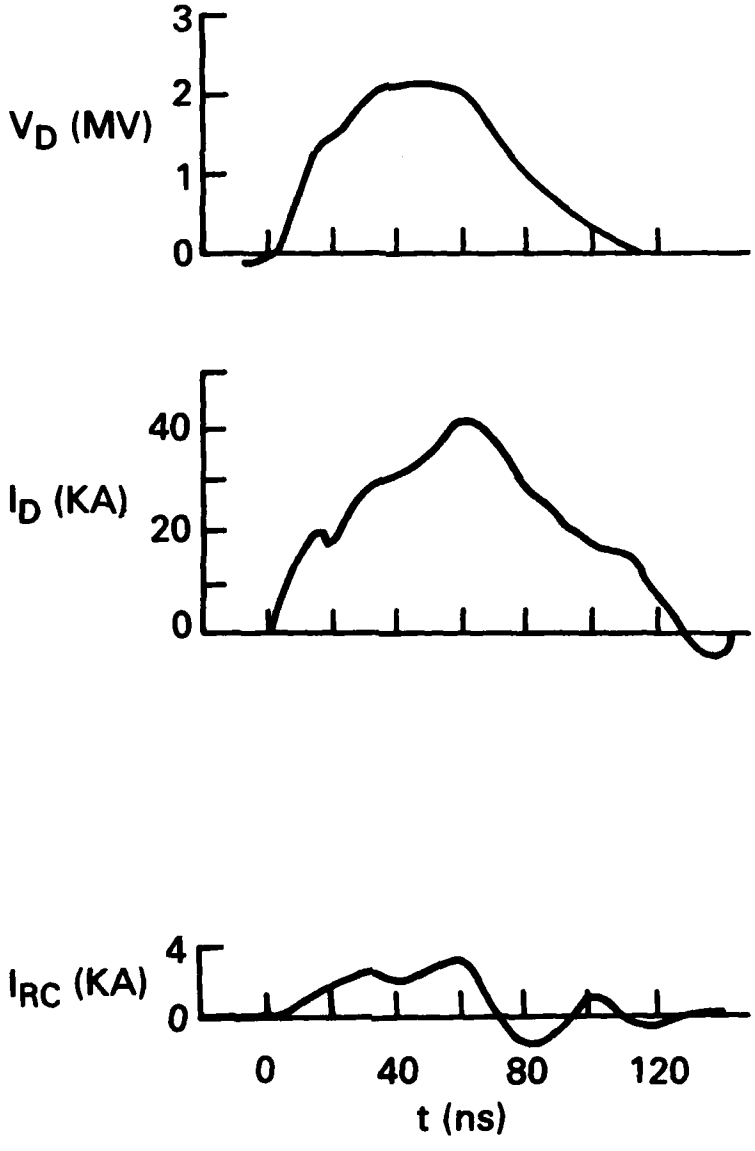

Figure 16 — Electrical parameters for the electron beam passing through a 1 cm aperture. V_D is the voltage measured on the diode voltage monitor, I_D is the current measured on the diode current monitor, and I_{RC} is the current measured on the Rogowski coil placed next to and on the atmosphere side of the carbon aperture.

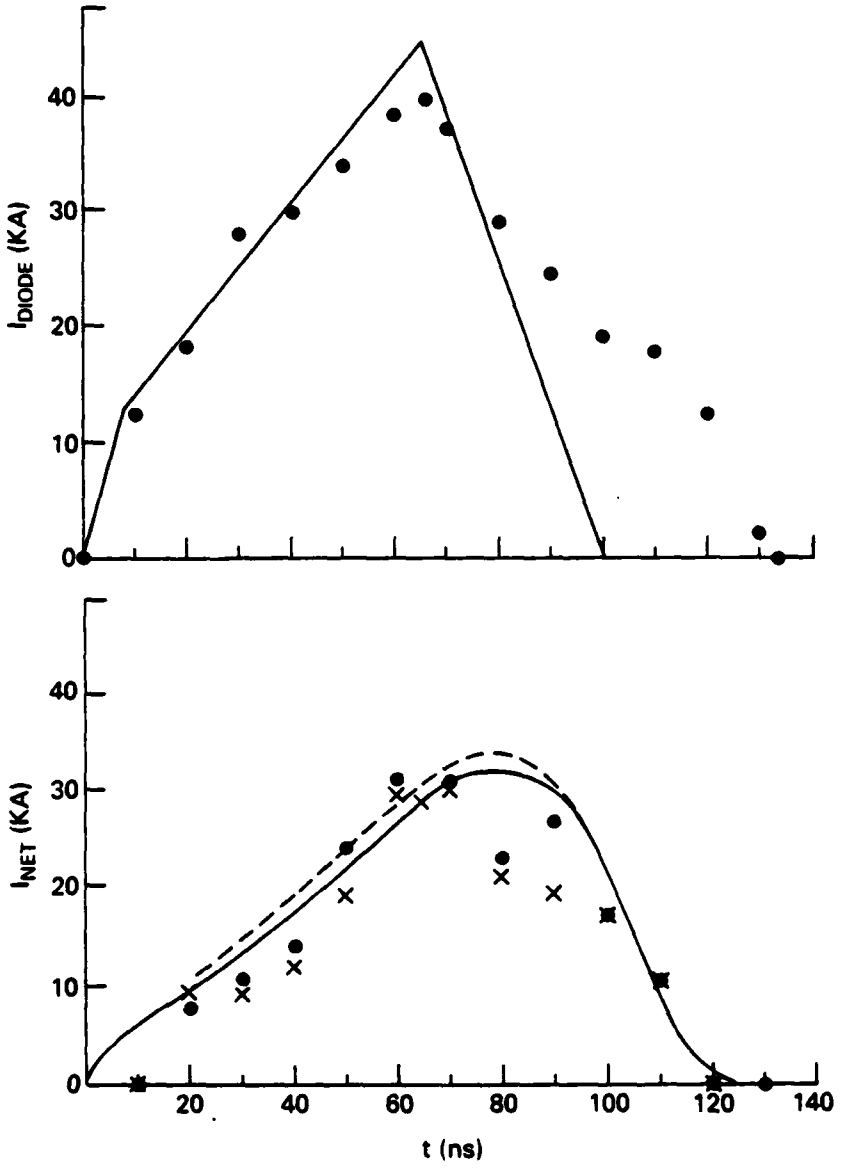

Figure 17 — Measured and calculated currents for the electron beam propagating "freely" in the atmosphere.

Top: ● points read from the measured diode current
——— a simple straight line model for the measured diode current.

Bottom: ● points read from the measured net current 15 cm from the foil.
x points read from the measured net current at the anode foil. (Net currents are measured with the Rogowski coil.)
——— calculated net current excluding N_4^+,
– – – – calculated net current including N_4^+.

Net currents are calculated using the simple lumped parameter circuit model of the propagating beam and the CHMAIR code[21] for air chemistry.

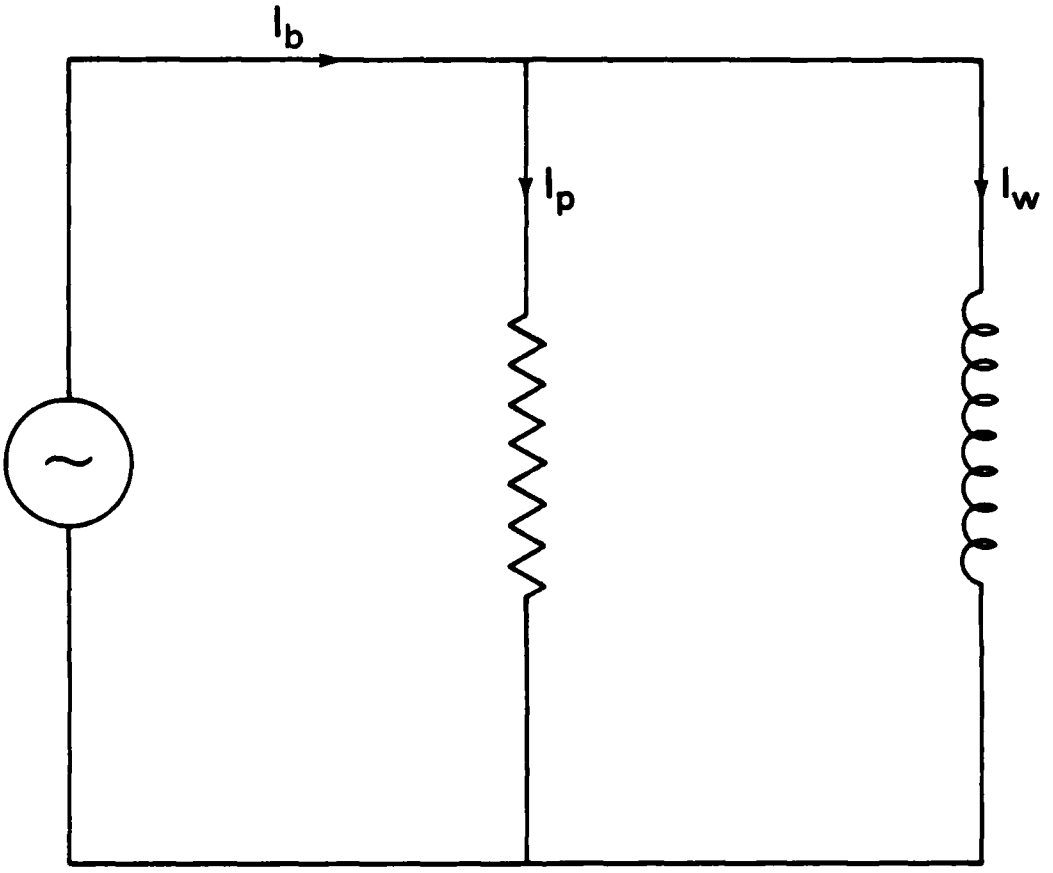

Figure 18 — A simple lumped parameter circuit model for a "freely" propagating electron beam. The generator is represented by a current source with current I_b which is the beam current. The conducting channel in the atmosphere created by the beam is represented by a resistive path back to the current source which carries the plasma current I_p. The remainder of the current I_w returns to the current source via the conducting screen around the box in which the beam is propagating or via deflections of the beam back towards the generator. These paths are mostly inductive because of the large radii involved.

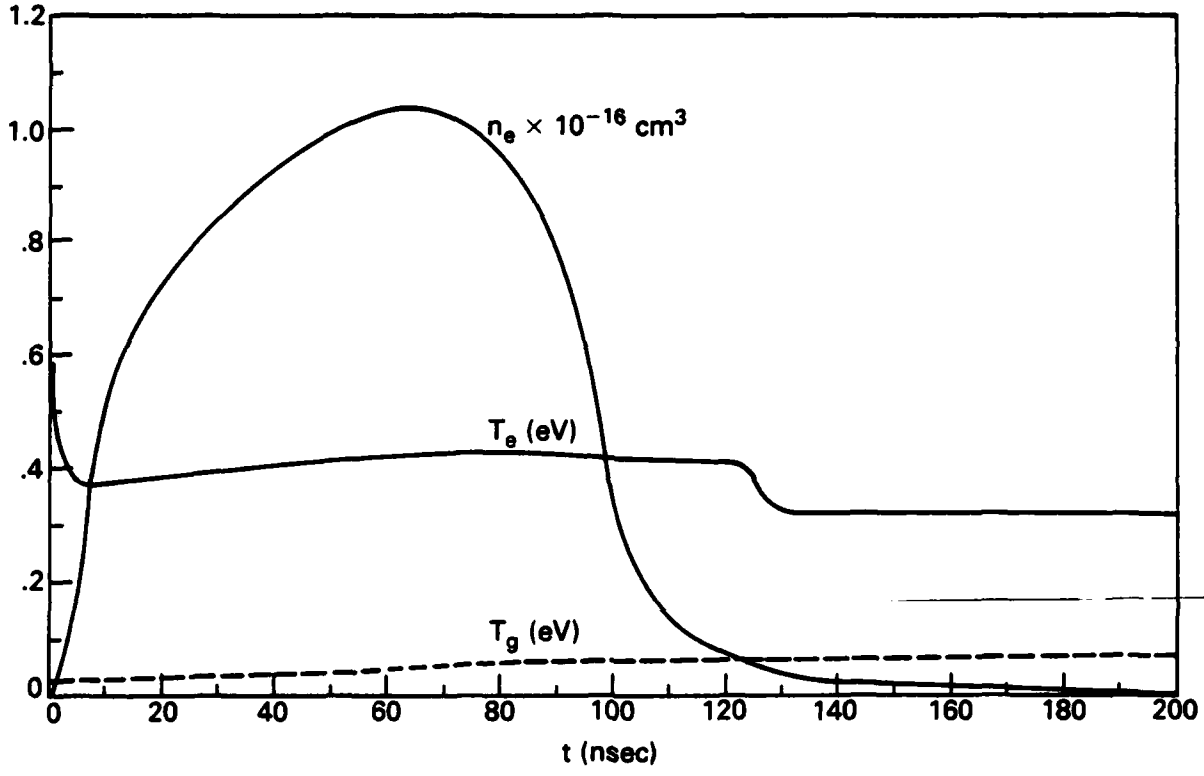

Figure 19 — Properties of air plasma created by the passage of the beam at −20 cm from the anode foil as calculated using the CHMAIR air chemistry code. n_e is the electron density, T_e is the electron temperature, and T_g is the gas kinetic temperature.

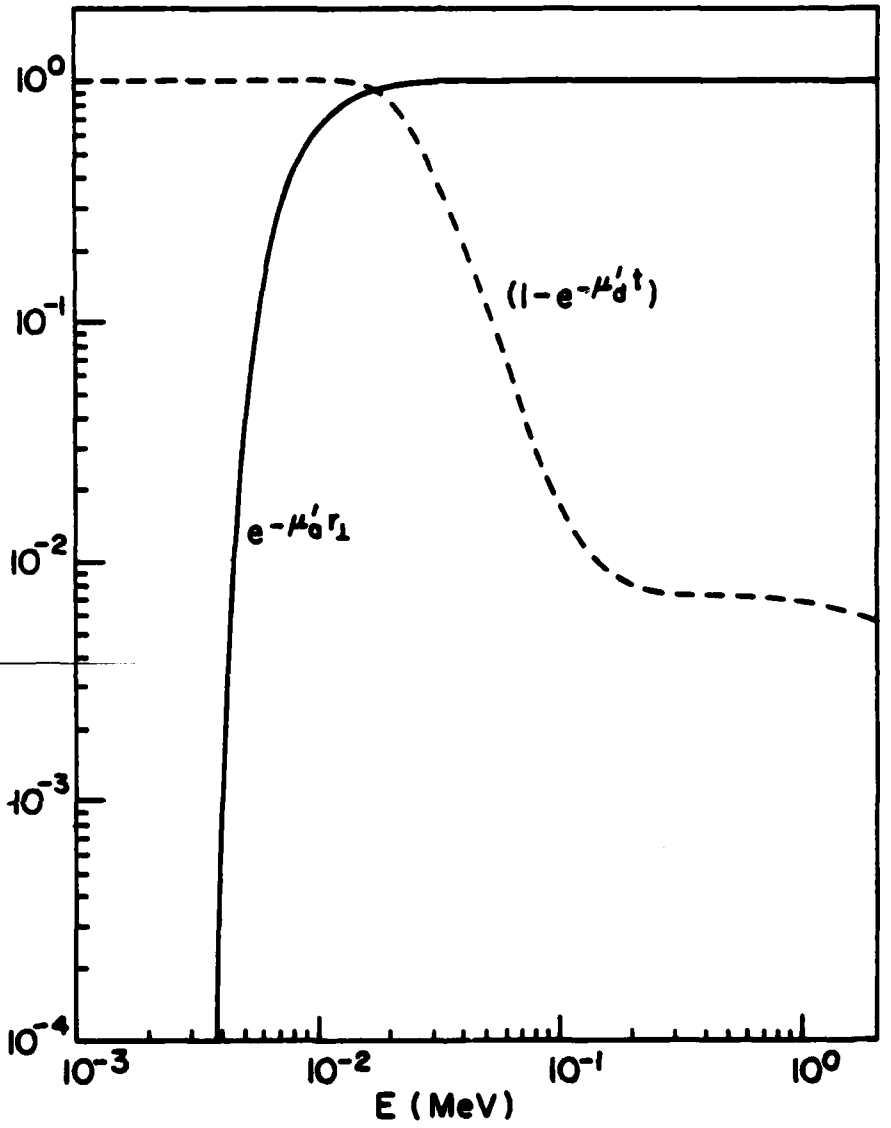

Figure 20 — Xray absorption and transmission curves.
——— transmission of air at S.T.P.
– – – – absorption of CaF_2.

DISTRIBUTION LIST

1. Commander
   Naval Sea Systems Command
   Department of the Navy
   Washington, D.C. 20363
   ATTN: NAVSEA 03H (Dr. C.F. Sharn)

2. Central Intelligence Agency
   P.O. Box 1925
   Washington, D.C. 20013
   ATTN: Dr. C. Miller/OSI

3. Air Force Weapons Laboratory
   Kirtland Air Force Base
   Albuquerque, New Mexico 87117
   ATTN: Lt. Col. J.H. Havey

4. U.S. Army Ballistics Research Laboratory
   Aberdeen Proving Ground, Maryland 21005
   ATTN: Dr. D. Eccleshall (DRXBR-BM)

5. Ballistic Missile Defense Advanced Technology Center
   P.O. Box 1500
   Huntsville, Alabama 35807
   ATTN: Dr. L. Harvard (BMDSATC-1)

6. B-K Dynamics Inc.
   15825 Shady Grove Road
   Rockvile, Maryland 20850
   ATTN: Mr. I. Kuhn

7. Intelcom Rad Tech
   P.O. Box 81087
   San Diego, California 92183
   ATTN: Mr. W. Selph

8. Lawrence Livermore Laboratory
   University of California
   Livermore, California 94550
   ATTN: Dr. R.J. Briggs
   Dr. T. Fessenden
   Dr. E.P. Lee

9. Mission Research Corporation
   735 State Street
   Santa Barbara, California 93102
   ATTN: Dr. C. Longmire
   Dr. N. Carron

10. National Bureau of Standards
    Gaithersburg, Maryland 20760
    ATTN: Dr. Mark Wilson

11. Science Applications, Inc.
1200 Prospect Street
LaJolla, California 92037
ATTN: Dr. M.P. Fricke
Dr. W.A. Woolson

12. Science Applications, Inc.
Security Office
5 Palo Alto Square, Suite 200
Palo Alto, California 94304
ATTN: Dr. R.R. Johnston
Dr. Leon Feinstein

13. Science Applications, Inc.
1651 Old Meadow Road
McLean, Virginia 22101
ATTN: Mr. W. Chadsey

14. Science Applications, Inc.
8201 Capwell Drive
Oakland, California 94621
ATTN: Dr. J.E. Reaugh

15. Naval Surface Weapons Center
White Oak Laboratory
Silver Spring, Maryland 20910
ATTN: Mr. R.J. Biegalski
Dr. R. Cawley
Dr. J.W. Forbes
Dr. D.L. Love
Dr. C.M. Huddleston
Mr. W.M. Hinckley
Dr. G.E. Hudson
Mr. G.J. Peters
Mr. N.E. Scofield
Dr. E.C. Whitman
Dr. M.H. Cha
Dr. H.S. Uhm
Dr. R.B. Fiorito

16. C.S. Draper Laboratories
Cambridge, Massachusetts 02139
ATTN: Dr. E. Olsson
Dr. L. Matson

17. M.I.T. Lincoln Laboratories
P.O. Box 73
Lexington, Massachusetts 02173
ATTN: Dr. J. Salah

18. Physical Dynamics, Inc.
P.O. Box 1883
LaJolla, California 92038
ATTN: Dr. K. Brueckner

19. Office of Naval Research
Department of the Navy
Arlington, Virginia 22217
ATTN: Dr. W.J. Condell (Code 421)

20. Avco Everett Research Laboratory
2385 Revere Beach Pkwy.
Everett, Massachusetts 02149
ATTN: Dr. R. Patrick
Dr. Dennis Reilly

21. Defense Technical Information Center
Cameron Station
5010 Duke Street
Alexandria, VA 22314 (12 copies)

22. Naval Research Laboratory
Washington, D.C. 20375
ATTN: M. Lampe — Code 4792
M. Friedman — Code 4700.1
J.R. Greig — Code 4763 (50 copies)
I.M. Vitkovitsky — Code 4770
T. Coffey — Code 4000
Superintendent, Plasma Physics Div. — Code 4700 (25 copies)
Library — Code 2628 (20 copies)
A. Ali — Code 4700.1T
D. Book — Code 4040
J. Boris — Code 4040
S. Kainer — Code 4790
A. Robson — Code 4760
M. Picone — Code 4040
D. Spicer — Code 4169
M. Raleigh — Code 4763
R. Pechacek — Code 4763
J.D. Sethian — Code 4762
K.A. Gerber — Code 4762
D.N. Spector — Code 4762

23. Defense Advanced Research Projects Agency
1400 Wilson Blvd.
Arlington, Virginia 22209
ATTN: Dr. J. Mangano
Dr. J. Bayless

24. JAYCOR
205 S. Whiting St.
Alexandria, Virginia 22304
ATTN: Drs. D. Tidman
R. Hubbard
J. Gillory

25. JAYCOR
Naval Research Laboratory
Washington, D.C. 20375
ATTN: Dr. R. Fernsler — 4770
Dr. G. Joyce — Code 4790
Dr. S. Goldstein — Code 4770

26. SAI
Naval Research Laboratory
Washington, D.C. 20375
ATTN: A. Drobot — Code 4790
W. Sharp — Code 4790

27. Physics International, Inc.
2700 Merced Street
San Leandro, CA
ATTN: Dr. J. Maenchen
Dr. E. Goldman

28. Mission Research Corp.
1400 San Mateo, S.E.
Albuquerque, NM 87108
ATTN: Dr. Brendan Godfrey

29. Princeton University
Plasma Physics Laboratory
Princeton, NJ 08540
ATTN: Dr. F. Perkins, Jr.

30. McDonnell Douglas Research Laboratories
Dept. 223, Bldg. 33, Level 45
Box 516
St. Louis, MO 63166
ATTN: Dr. Michael Greenspan

31. Cornell University
Ithaca, NY 14853
ATTN: Prof. David Hammer

32. Sandia Laboratories
Albuquerque, NM 87185
ATTN: Dr. Bruce Miller
Dr. Barbara Epstein
Dr. John Olsen
Dr. Don Cook

33. University of California
Physics Department
Irvine, CA 92717
ATTN: Dr. Gregory Benford

34. Naval Air Systems Command
Washington, D.C. 20361
ATTN: Dr. R.J. Wasneski, Code AIR-350F

35. Beers Associates, Inc.
P.O. Box 2549
Reston, VA 22090
ATTN: Dr. Douglas Strickland

36. U.S. Department of Energy
Washington, D.C. 20545
Office of Fusion Energy, ATTN: Dr. W. F. Dove
Office of Inertial Fusion, ATTN: Dr. T. Godlove

37. AFOSR/NP
Bolling Air Force Base
Washington, D.C. 20331
ATTN: Capt. R.L. Gullickson